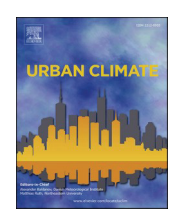


Contents lists available at ScienceDirect

Urban Climate

journal homepage: www.elsevier.com/locate/uclim





Urban greenness and its cooling effects are influenced by changes in drought, physiography, and socio-demographics in Los Angeles, CA

Dion Kucera*, G. Darrel Jenerette

Department of Botany and Plant Sciences, University of California, Riverside, Riverside, CA, USA

ARTICLE INFO

Keywords: Land surface temperature Luxury effect Standardized Precipitation Evapotranspiration Index Urban forest Urban vegetation Vegetative cooling

ABSTRACT

The multidecadal change in urban microclimate and greenness, particularly in response to drought and a warming climate, has implications for urban residents' well-being. Urban greenness, temperature, and vegetative cooling vary spatially. However, the dynamics of the relationships among these variables and their influencing factors are poorly characterized. Using the Los Angeles Urban Region, USA as a case study we evaluate the dynamics among urban vegetation and climate through an evaluation of satellite-based observations between 1985 and 2021. We hypothesize that microclimate changes are driven by water demand and aridity, with increasing aridity enhancing transpiration and vegetation-cooling, but that irrigation variation, assessed through proxy demographic variables of income modify water availability. Our results show that the L.A. region warmed by 0.13 °C/year, NDVI increased annually by 4.81 \times 10 $^{-4}$, and vegetative cooling increased by 0.08 °C/NDVI/year. A consequence of these dynamics was that the luxury effect of income as a mediator of NDVI and LST declined 41% and 28%, respectively, between 1990 and 2020. The changes in urban microclimates over time and from drought are affected by social and physiographic variables associated with water availability and water demand and are increasingly leading to less racially equitable neighborhood distributions of heat.

1. Introduction

In arid and semi-arid cities, neighborhood temperature and vegetation distributions are generally coupled spatially, but these variables' dynamics are not well understood (Qi et al., 2022; Cheng et al., 2023). Urban environmental dynamics may reflect both responses to global climate changes (Varquez and Kanda, 2018) as well as more local land management actions, notably tree planting and irrigation (Jin et al., 2019). Both climate changes and management decisions may interact in their effects on neighborhood greenness and temperature (Yuan and Bauer, 2007; Jenerette et al., 2011; Ziter et al., 2019). The dynamics of urban environments lead to altered availability of both greenspace and heat risks. Further, variability in the effects of global and regional changes to urban microclimate conditions may be moderated by the built environment, physiography, and demographic distributions which may cause additional spatially varying trajectories of urban environments (Oke and Stewart, 2012; Coseo and Larsen, 2014) and likely will have consequences for societal equity. Thus, while urban neighborhood greenness and temperatures are likely changing, the magnitude, drivers, and impacts of urban variation in these changes are not well resolved.

^{*} Corresponding author at: Department of Botany and Plant Sciences, University of California Riverside, Riverside, CA 91521, USA. *E-mail address*: dion.kucera@email.ucr.edu (D. Kucera).

Hydrologic changes in urban environments are directly tied to urban greenness and temperature dynamics (Qiu et al., 2013; Konarska et al., 2016; Litvak et al., 2017). Transpiration, dependent on both water availability and atmospheric demand, is a major component of neighborhood cooling by vegetation (Chen et al., 2019; Winbourne et al., 2020; Zhao et al., 2020). During drought, urban vegetative cooling may exhibit distinct shifts due to changes in the spatial availability of water and atmospheric evaporative demand. This is particularly true in many arid and semi-arid cities where irrigation plays a pivotal role in the availability of water for the urban ecosystem (McCarthy and Pataki, 2010; Pataki et al., 2011b; Liang et al., 2017). Irrigation modifies local temperatures, evaporative demand, and plant transpiration via an increase in water availability (Vahmani and Hogue, 2015; Gao et al., 2020) and humidity (Broadbent et al., 2018; Mishra et al., 2020), potentially decoupling greenness and temperature dynamics from precipitation (Jenerette et al., 2013; Winbourne et al., 2020; Ibsen et al., 2023). Further, drought often co-occurs with hotter temperatures and higher vapor pressure deficit (VPD; (Grossiord et al., 2020), suggesting the variables that increase temperature or aridity may increase vegetative cooling during drought via increased evaporative demand. Although observations for individual droughts have noted the failure of urban irrigation to prevent greenness declines and temperature increases (Quesnel et al., 2019; Miller et al., 2020; Allen et al., 2021), these studies offer only a snapshot of an evolving temporal relationship between aridity, irrigation, and urban greennesstemperature dynamics. The urban water deficit hypothesis poses uncertainty about how urban ecosystems react to sustained aridity over time. While understanding the long-term impacts of urban aridity is outside the scope of individual drought analyses, the dynamics of greenness and temperature in response to aridity have not been assessed at a multidecadal scale.

Physiographic factors may also moderate the drivers in neighborhood greenness and temperature dynamics. Coastal regions are cooler and have a lower VPD than inland regions (representing a coast-to-inland maritime gradient), elevation is associated with decreased temperatures and VPD (Li et al., 2021), and impervious cover increases sensible heat flux, increasing VPD (Zipper et al., 2017). However, VPD may not be the proximate driver of transpiration: VPD drives transpiration in water-limited sites, but solar radiation drives transpiration in energy-limited sites (Whitley et al., 2013). Therefore, the coastal marine layer, in decreasing photosynthetically active radiation (PAR), and impervious cover, in increasing temperature, may also have a role in mediating the relationship between vegetative cooling, plant greenness, and temperature. Beyond these physiographic factors, socioeconomic distributions may further modify the dynamics between urban greenness and temperature.

Social variables influence urban temperatures (Huang et al., 2011), water availability (Corral-Verdugo et al., 2003), and greenness (Schwarz et al., 2015). The luxury effect describes how wealthy regions of a city have greater greenness and are cooler than less affluent regions (Harlan et al., 2006; Leong et al., 2018; Wetherley et al., 2018; Barrera et al., 2019; Shih, 2022). These demographic drivers may similarly influence the dynamics of neighborhood vegetation and temperature although how these effects occur is uncertain. While affluent neighborhoods might consume more water post-drought (Balling et al., 2008; House-Peters et al., 2010), strengthening the luxury effect, water restrictions could cause these areas to reduce irrigation, potentially weakening the effect. Through time greenness may have increased in response to municipal tree planting campaigns (Eisenman et al., 2021) such as MillionTreesNYC (McPhearson et al., 2010) and the Greening the Gateway Cities Program in Massachusetts (Breger et al., 2019). However, tree planting campaigns have been observed to increase tree cover in high tree-cover regions, perpetuating racial tree cover disparities (Krafft and Fryd, 2016; Garrison, 2017, 2018) and increasing the luxury effect. These patterns associated with wealth and demographics intersect with the luxury effect, emphasizing the importance of understanding how it may change through time.

The luxury effect itself may vary over time, potentially hindering individuals' ability to manage the urban heat and greenscape (Zhou et al., 2011). This instability may be compounded by race-specific characteristics that introduce additional complexity to the luxury effect's dynamics (Watkins and Gerrish, 2018; Venter et al., 2020). For instance, even after controlling for income, racial minorities have been found to experience higher temperatures compared to their non-Hispanic White counterparts (Hoffman et al., 2020; Benz and Burney, 2021). Furthermore, while affluence tends to promote increased greenness in predominantly White neighborhoods, Black and Asian neighborhoods demonstrate a different pattern, with low-income communities showing a greater likelihood of increased greenness (Huang et al., 2011). Increased affluence among minority communities can sometimes lead to a decrease in greenness, contradicting the trend observed in White neighborhoods and suggesting race-specific differences in how urban residents manage greenness (Casey et al., 2017). To better reflect the influence of race on mediating urban greenness and temperature (Jesdale et al., 2013; Locke and Grove, 2014), the non-stationarity of race-dependent relationships should be assessed. The impact of race on greenness and temperature can vary over time and by race, potentially magnifying disparities in well-being (Clarke et al., 2014). This dynamic, race-mediated influence of income on greenness and temperature, may exacerbate disparities in well-being across neighborhoods with predominantly different racial demographics (Morello-Frosch et al., 2011).

To address the uncertainties in the spatial and temporal distributions of urban greenness and temperature we evaluated their dynamics over 37 years throughout the semi-arid, irrigated Greater Los Angeles, USA urban region (LAUR). Using LAUR as a case study we ask: How have urban surface temperatures and the distribution of vegetation changed over 1985–2021 in the greater Los Angeles region? We answered our research question by evaluating the magnitude and possible drivers of changes in neighborhood greenness, temperature, and the effect of vegetation on temperatures throughout the LAUR between 1985 and 2021. We tested the prediction that urban greenness and temperature increased over time due to tree planting campaigns and climate change, respectively, and that vegetative cooling has increased due to global increases in temperature and aridity. We evaluated an urban water deficit hypothesis to identify whether long-term changes in greenness and temperature are associated with the relative distribution of water availability. We tested the prediction that greenness declines, temperature increases, and vegetative cooling increases with increasing drought. We also tested the prediction of large neighborhood variation in the dynamics of greenness and temperature and that this neighborhood variation would be related to both physiographic and income differences among neighborhoods. As an outcome of the dynamics in neighborhood greenness and temperature, we evaluated the dynamics of their social equity throughout the region to assess the changing availability of greenness and heat throughout the region. By quantifying the change in urban greenness, temperatures, and

vegetative cooling over a multidecadal timescale we describe how physiographic and social variables modify urban vegetation dynamics in a model city.

2. Methods

2.1. Study area

All data were averaged to the census tract before analysis, other than the Standardized Precipitation Evapotranspiration Index, which has one data point per month for the study area. The census tract was chosen as the scale of analysis consistent with censusprovided data and is sufficiently large to provide robust demographic data (Wong and Sun, 2013). Over the temporal span of this study, the study area had a mean NDVI of 0.25, a mean LST of 35 °C, and an average of 34.8 cm rain year -1. LAUR has unique characteristics making it a useful model city for this study. The LAUR is one of two megacities in the United States, located on the southwestern coast with a Mediterranean climate (Köppen Csa and Csb). Within the LAUR neighborhood per capita median income varies from \$9000 to over \$250,000 per year, while racial diversity is one of the greatest in the nation. LAUR's socio-economic diversity contributes to inequities in the distribution of heat and urban greenness (Schwarz et al., 2015; Tayyebi and Jenerette, 2016; Yin et al., 2023). To partially rectify this, Los Angeles planted 69,776 trees between 2007 and 2014 as part of the Million Trees L.A. initiative, focusing new plantings in regions with non-white residents (Garrison, 2018). As almost all of LAUR's urban trees are nonnative (Gillespie et al., 2016; Jenerette et al., 2016), they require extensive management. Further, the region's physiography is unique for large cities in the United States, where temperature and aridity increase along a maritime climate gradient from the coast to the San Gabriel Mountains ~48 km inland. LAUR also experiences frequent drought both annually (due to the Mediterranean semi-arid weather) and inter-annually. Regionally, patterns of urban greenness are closely associated with rates of evaporation, highlighting the importance of irrigation in a region where summertime rainfall accounts for only 13% of evapotranspiration (Pataki et al., 2011a; Bijoor et al., 2012; Liang et al., 2017). Urban trees in the LAUR can use a large amount of water for transpiration (Pataki et al., 2011a), which may make LAUR's urban forest susceptible to drought as trees in the LAUR, particularly those that are shallowly rooted, may supplement their water needs with rainfall (Bijoor et al., 2012). During the 2012–2016 California megadrought, urban green cover mediated drought-induced heat waves via vegetative cooling, albeit reduced from pre-drought levels (Allen et al., 2021).

Our study area covers 3474 km² of urbanized land cover in the Greater Los Angeles, California urban region (LAUR [Fig. 1]). Most of the area is within Los Angeles County, however, about a quarter of the urban extent is within Orange and San Bernardino Counties. We defined the extent of the study region by 2010 census tract boundaries that overlay non-mountain populated areas of the greater Los Angeles region. Census tracts in the mountains (e.g., Santa Monica, San Gabriel) or that otherwise contained less than ~50% urbanized land cover were removed, as were tracts with no or very little population (such as around the airport or industrial centers). We used all populated, non-mountain census tracts within the boundaries of the Landsat tile centered over Los Angeles, yielding 2794 tracts. In 1990, the first year of census data utilized, the LAUR had a population of 10,880,125 and an average density of 4150 people km⁻². By the end of the time series at the 2020 census the LAUR's population had increased 15% percent to 12,498,697 whereas density increased 23% percent to 5098 people km⁻².

2.2. Changes in urban greenness and land surface temperature

We assessed the distribution of vegetated cover and land surface temperature using the Landsat 4, 5, 7, and 8 satellites collected from all months from 1985 through the end of 2021. The Landsat satellites pass over the LAUR in the morning between approximately

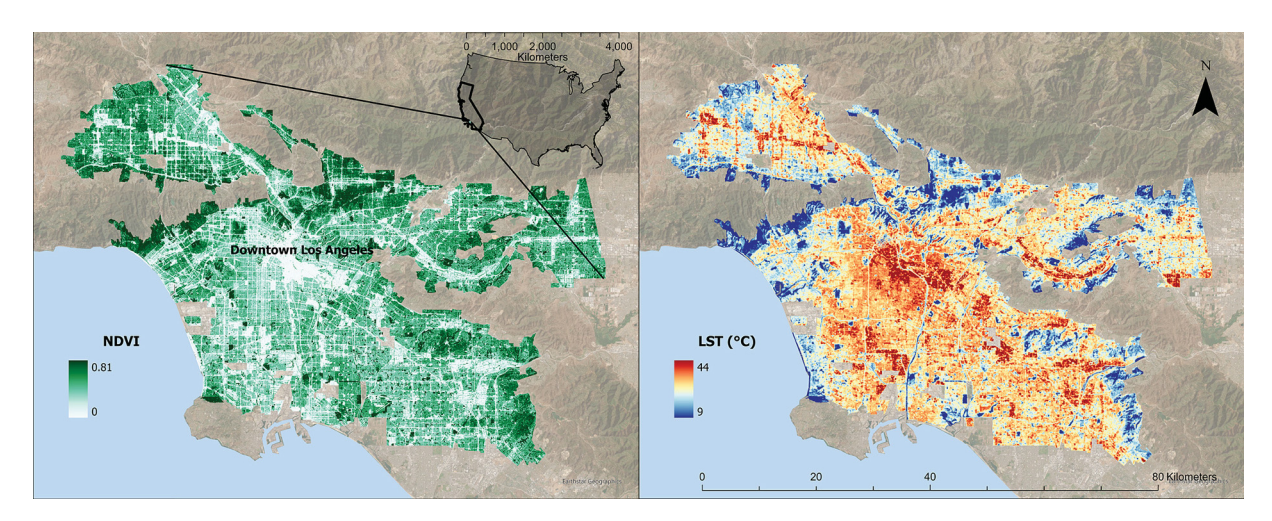


Fig. 1. The study area encompassed the Greater Los Angeles, California urban region (LAUR). Using a long-term mean of Landsat imagery from 1985 to 2021, the hottest regions were those that had the lowest plant greenness.

16:00 and 18:00 GMT (8:00–10:00 PST). The individual Landsat satellites have a 16-day return interval, however, subsequent satellites (e.g., Landsat 7 vs. Landsat 8) are in an eight-day offset orbit, providing greater temporal fidelity. Landsat is provided at 30 m² resolution as captured natively (visible bands) or via resampling (thermal bands). Landsat has the longest publicly-available satellite record of Earth observation (Loveland and Dwyer, 2012) and has been used for urban research for decades, including to estimate urban vegetative cover, microclimate, and their relationships (Buyantuyev et al., 2007). We relied on the Collection-2 Analysis Ready Data (ARD) product, provided by the United States Geological Survey (USGS) and accessed from Earth Explorer (Dwyer et al., 2018). The ARD product is atmospherically corrected and radiometrically calibrated by the USGS using a standardized approach to make the data from the different Landsat satellites directly comparable to one another, facilitating comparative analyses (Banskota et al., 2014; Zhu, 2019) and making it suitable for time series analysis (Zhu, 2019).

All data were pre-processed in MATLAB r2021b and ArcGIS Pro 2.9. To ensure the highest quality data we only downloaded Landsat tiles that contained <10% cloud cover. Further, we did not use Landsat 7 after May 31st, 2003, following the failure of the satellite's scan line corrector. The subsequent striping of Landsat 7 imagery, coupled with cloud masking, yielded a limited number of usable pixels and produced unreliable results. Therefore, we have no data from December 2011–March 2013, representing the gap between Landsat 5 and Landsat 8. All non-clear pixels (clouds, water, aerosols, etc.) were masked in MATLAB to take advantage of parallel processing. Images that were not usable following cloud masking (e.g., contained too few pixels) were manually discarded following visual inspection yielding a final stack of 215 images. The masked TIFF files were then imported to ArcGIS Pro where they were clipped to the study extent (Fig. 1). The data were then averaged at the census tract scale using 1990, 2000, 2010, and 2020 census tract boundaries. The TIFF imagery was finally re-uploaded to MATLAB where the data were averaged to the monthly scale, generating a data product consistent with the monthly scale of the weather and drought datasets.

From the Collection-2 ARD dataset, we derived the Normalized Difference Vegetation Index (NDVI), a commonly used proxy for vegetation cover (Carlson and Ripley, 1997) or biomass (Borowik et al., 2013). NDVI, which ranges from -1 to +1, takes advantage of chlorophyll's reflectivity in the near-infrared but absorption in the red portion of the electromagnetic spectrum, where values closer to +1 indicate greater vegetated cover and values less than zero are unvegetated (Pettorelli et al., 2011; Esau et al., 2016; Huang et al., 2020). For the LAUR we found that pixels with a Landsat NDVI of 0.1 have 1% green cover. We derived this value by randomly selecting images from across the time series, randomly identifying individual pixels within those images, and then demarcating the vegetated area of those pixels using the sub-meter World Imagery from ArcGIS. To remove unvegetated pixels we excluded all pixels with an NDVI<0.1 before analysis, consistent with previous studies using locally assessed thresholds (Esau et al., 2016; Liu et al., 2018). Few pixels transitioned between the 0.1 threshold over the time series: between the start and end of the time series the number of "vegetated" pixels with an NDVI>0.1 increased by 1.52%. The LST dataset was not similarly modified.

To assess the change in land surface temperature we used the Surface Temperature product from the Collection-2 ARD dataset. ARD LST is derived using the single-channel algorithm based on the thermal band while accounting for both atmospheric effects and surface emissivity, although Landsat 8–9 utilizes the LaSRC algorithm (USGS, 2021b) whereas Landsat 4–7 utilize the LEDAPS algorithm (USGS, 2021a). These algorithms use the radiative transfer equation, incorporating emissivity corrections based on NDVI values to account for the distinct emissivity of vegetation compared to other surfaces. USGS processes the ARD LST by applying atmospheric compensation to the thermal bands, which adjusts for the effects of water vapor and other atmospheric gases, ensuring accurate ground temperature readings. The resolution of surface temperature varies by satellite: Landsat 4–5 are at $120 \, \mathrm{m}^2$, Landsat 7 is at $60 \, \mathrm{m}^2$, and Landsat 8 is at $100 \, \mathrm{m}^2$, however, all data were resampled by USGS to $30 \, \mathrm{m}^2$. The thermal images are collected at the same time as the visible bands that go into the derivation of NDVI, making the stack of LST and NDVI images the same size. The ARD Surface Temperature product, provided in Kelvin, is similarly comparable between satellites in the Landsat series (Cook et al., 2014); the standardization of the LST ARD processing makes it appropriate for time series analysis.

2.3. Changes in LST-NDVI

Using our 215-image dataset allowed us to quantify variability in LST-NDVI. Vegetative cooling, defined as the slope of the LST-NDVI relationship, is used as a proxy for drought in non-urban landscapes in indices such as the Vegetation Temperature Condition Index (VTCI; Wan et al., 2004), the Vegetation Supply Water Index (VSWI; Cunha et al., 2015), and the modified Temperature Vegetation Drought Index (mTVDI; Zhao et al., 2017). To determine the temporal change in the cooling provided by urban plants we linearly regressed average monthly NDVI against average monthly LST, where the slope represents the cooling provided by plants in °C/NDVI and the intercept represents the bare-soil surface temperature. We evaluated this regression for each date in the time series to create a new array showing the change in LST-NDVI through time.

2.4. Weather datasets and the Standardized Precipitation Evapotranspiration Index (SPEI)

We used weather data from TerraClimate, a $\sim 4~\rm km^2$ global multidecadal weather dataset (Abatzoglou et al., 2018). From TerraClimate we acquired actual evapotranspiration, climate water deficit, potential evapotranspiration, precipitation accumulation, solar radiation, minimum temperature, maximum temperature, vapor pressure, and vapor pressure deficit. We accessed TerraClimate (IDAHO_EPSCOR/TERRACLIMATE) using Google Earth Engine (GEE), a cloud-based petabyte-scale GIS (Gorelick et al., 2017). We downloaded weather data from GEE for the LAUR from 1984 through the end of the time series, allowing us to derive new variables of 1–12 months of cumulative precipitation for each month. As with the Landsat imagery, we averaged the TerraClimate data in ArcGIS Pro to our 2010 census tract boundaries before uploading the averaged data to MATLAB for analysis. In addition to TerraClimate, the climatic water balance was an important variable in our study.

4

We quantified drought using the Standardized Precipitation Evapotranspiration Index (SPEI), as provided by SPEIbase v2.7 (Vicente-Serrano et al., 2010). The SPEI, initially proposed by Vicente-Serrano et al. (2010), considers both precipitation and temperature-derived potential evapotranspiration, making it notably sensitive to climatic changes. This approach provides a series where negative values signify drought conditions and positive ones indicate wetter-than-average periods. The SPEI is commonly used in ecological research as a measure of drought, overcoming limitations of the similarly derived standardized precipitation index in its inclusion of both temperature and potential evapotranspiration (Vicente-Serrano et al., 2010). SPEI values further from zero indicate increasingly wet (positive) or dry (negative) periods relative to the long-term average. A unique feature of the SPEI relative to other drought indices is that data are aggregated at monthly scales. For instance, a 3-month SPEI of 0.64 for June indicates that the June of interest is 0.64 standard deviations wetter than the average of all April–June periods in the time series used to generate the SPEI. At intra-annual scales, monthly aggregations help to overcome the effect of seasonality in rainfall. Inter-annual aggregations are useful to quantify the effects of long-term drought. We used all monthly aggregations provided by SPEIbase from SPEI-1 through SPEI-48.

Drought is defined by SPEI values ≤ -0.5 (mild drought), while wet periods have an SPEI ≥ 0.5 (Feng et al., 2020). The more negative the value, the greater the deficit in precipitation/potential evapotranspiration. For this study, we defined drought as having an SPEI ≤ -1 (moderate drought), with wet periods having an SPEI $\geq +1$. The standardization of SPEI ensures that its values are directly comparable both across different locations and over various time periods. This makes SPEI an ideal tool for time series analysis, especially when incorporating seasonal variations (Vicente-Serrano et al., 2010). Using the monthly indices of when "dry" and "wet" periods occur, we created mean "dry" and "wet" variables for NDVI, LST, and LST-NDVI for each SPEI monthly aggregation.

2.5. Socio-demographic and physiographic variables

Census-tract level socio-economic data were obtained for each decennial census from 1990 to 2020. To minimize information loss when comparing relationships across time we used the census tract boundaries consistent with that year's data. When assessing mean

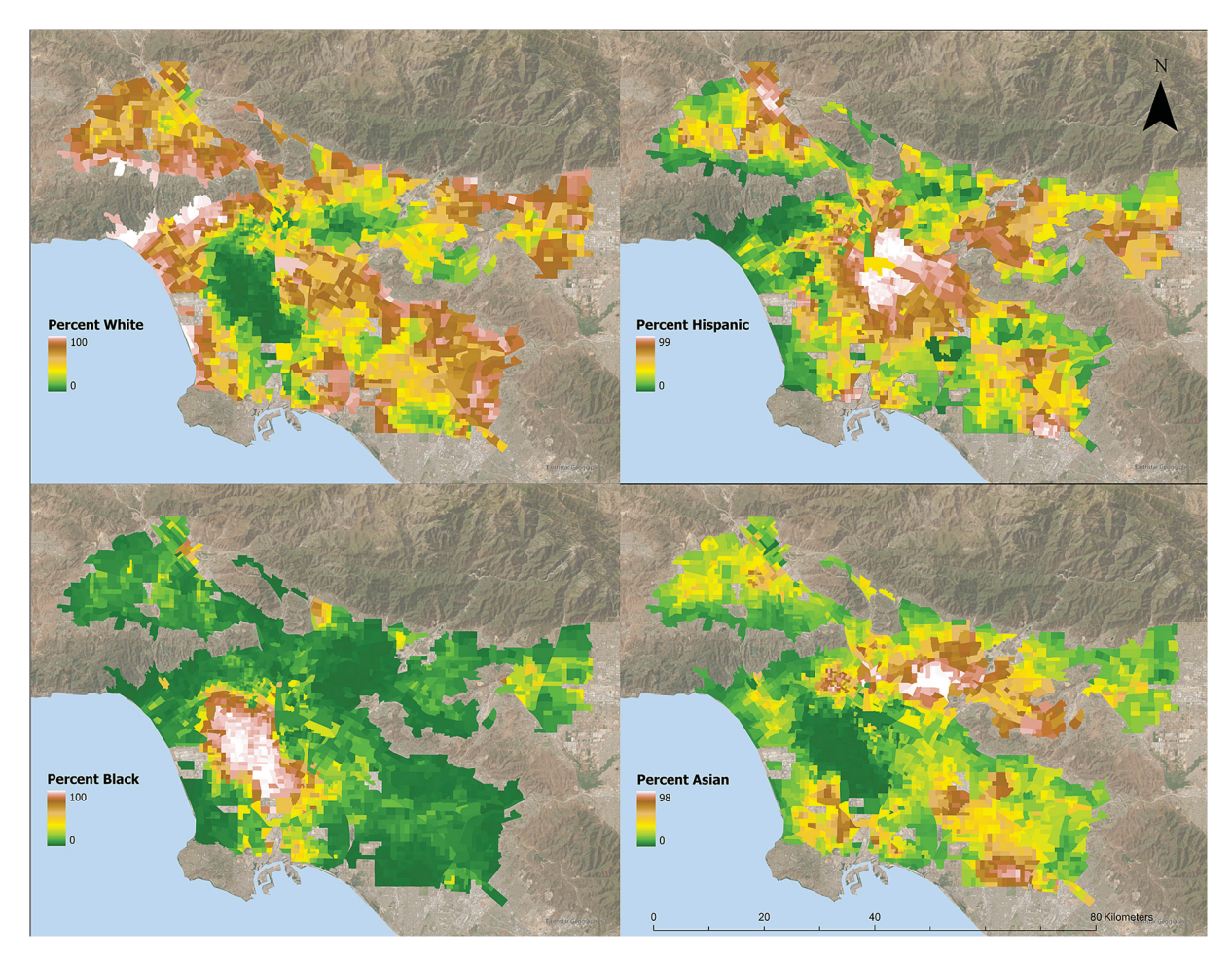


Fig. 2. The census tract distribution by race is heterogeneous, with per-race agglomerations. White communities are most common along the foothills, Hispanic communities are predominantly found around downtown Los Angeles, Black communities are west of downtown L.A., and Asian communities are found north of downtown near the city of Industry. Data are based on the 2010 census.

change in our variables in response to SPEI we used the 2010 census tract boundaries, as this is the only census tract year with associated tree canopy cover data. We derived population density by dividing the population of each census tract by that census tract's area. We also determined the racial composition of each census tract by dividing the population of White, Hispanic, Black, and Asian persons per census tract by the census tract's total population. The distribution of races within the LAUR is spatially heterogeneous, but there are race-specific agglomerations (Fig. 2). Other census variables we used were percent graduate degree holders per census tract, median household income, per-capita income, and income by race. We categorized census tracts by racial population using census datasets which denote the census-tract population of a given race as well as providing race-based income metrics; race-based census tract data utilized in this study were provided directly from the United States Census Bureau. These census datasets allowed us to use the percent of a given racial population per census tract as a dependent variable in regression analysis. Census data for 2000, 2010, and 2020 were obtained from data.census.gov. Data for 2000 is derived from the decennial census, while data for 2010 and 2020 are derived from the decennial census and the American Community Survey 5-year Estimates. Relevant tract-level census data for 1990 was found hosted by the Centers for Disease Control at https://www2.cdc.gov/nceh/lead/census90/house11/download.htm. Boundaries of census tracts for all years were obtained from https://www.census.gov/geographies/mapping-files.html. Census tract boundaries were used to manipulate the predictor variables.

The physiographic variables we evaluated included distance from the coast, elevation, percent impervious cover per tract, and percent tree canopy cover per tract. We created the distance from the coast variable in ArcGIS Pro by finding the distance from the Pacific Ocean to the centroid of the respective 1990–2020 census tract boundary. Visual inspection ensured irregularly shaped tracts did not lead to more than one centroid per tract. Elevation, acquired using GEE, came from the Shuttle Radar Topography Mission (SRTM) provided at a spatial resolution of 1-arc-second and a vertical accuracy of ± 6.87 m (Elkhrachy, 2018). It is important to note that in the LAUR "high elevation" connotes a few hundred meters; the median elevation is 80 m. Low elevation regions \leq 25th percentile range from sea level up to 34 m, whereas high elevation regions \geq 75th percentile are \geq 204 m. Both percent impervious cover and percent tree canopy cover came from the National Land Cover Database (NLCD). We used NLCD impervious cover for 2001 (to match the 2000 census), 2011 (2010 census), and 2021 (2020 census). We used only one data point for tree canopy cover, tying the 2011 NLCD tree canopy cover with the 2010 census. Finally, we also used the change in NDVI (either through time or during drought) as an independent variable to explain the change in LST. All datasets used in this study are described in Table 1.

To assess the effect these variables had on the change in NDVI and LST during drought we used bivariate linear regression in MATLAB, where Δ NDVI and Δ LST (wet-dry) were the dependent variables. Further, to assess the change in these variables through time we ran a pixel-by-pixel temporal linear regression of NDVI and LST in MATLAB. Our approach to determining the NDVI-Precipitation slope followed the same structure. For this temporal regression, we isolated the slope coefficient and used this term as a dependent variable in a new regression designed to explain the spatial variability of the NDVI and LST trends.

We explained the spatial variability of the per-pixel NDVI and LST trends through time by using structural equation modeling (SEM). SEM is a statistical approach used to test hypotheses about the relationships among observed and unobserved variables. SEM allows for the exploration of complex relationships, including those that are direct, indirect, and reciprocal (Wu et al., 2021; Manavvi and Rajasekar, 2023). In multiple regression, nearly all explanatory variables significantly explain variation in the dependent variables due to a large sample size of census tracts leading to p-values lower than 0.05 (Lantz, 2013). We only kept variables that had a partial r^2 of at least 0.05 in multiple regression.

3. Results

3.1. Spatiotemporal dynamics of NDVI, LST, and LST-NDVI

Initial analyses confirmed the expectation that the average NDVI and LST across the time series are well correlated spatially (pearson's r = -0.80, p < 0.001), such that the hottest urban regions are also those which are least vegetated (Fig. 1). Spatial variation

Table 1
Descriptive characteristics of all datasets used in the study. Census datasets are from 2010 for reference, but census data from 1990, 2000, 2010, and 2020 were utilized.

Dataset	Data utilized	Provider	Spatial resolution	Temporal resolution
Landsat Analysis Ready Data TerraClimate Shuttle Radar Topography Mission (SRTM)	NDVI and LST All Weather Variables Elevation	USGS Earth Explorer University of California, Merced NASA/USGS/JPL-Caltech	30-120 m ² 1/24th degree (~4 km) 1 arc sec (~30 m ²) with <7 m vertical accuracy	8–16 days Monthly
SPEIbase	Standardized Precipitation Evapotranspiration Index	Global SPEI Database v2.7	0.5° (~46 km for LAUR)	Monthly
National Landcover Data Base	Tree Cover, Impervious Cover	Multi-Resolution Land Characteristics consortium	$30m^2$	Decadal
P1, P9 (2010)	Demographic variables of race and population	United States Census Bureau	Census Tract	Decadal
S1901, S1903, S1501, B19301 (2010)	Social Variables of income and education	United States Census Bureau	Census Tract	Decadal
TIGER/Line® Shapefiles	Census Tract Boundaries	United States Census Bureau	Census Tract	

in the long-term average for NDVI and LST is itself associated with income and the built environment. In multiple regression, impervious cover and tree canopy cover explained 87% of the spatial variability of NDVI, where the effect of impervious cover on NDVI was 63% greater than that of tree cover (Supplemental Fig. 1). Every 10% increase in impervious cover was associated with a decrease in NDVI by 0.041 (*p*-value<0.001), while every 10% increase in tree cover was associated with an increase in NDVI of 0.0047 (*p*-value<0.001). Similarly, impervious cover and income explained 69% of the spatial variability of LST (Supplemental Fig. 2), with these variables increasing and decreasing LST, respectively. Impervious cover had an effect 59% greater on the spatial variation of LST than income. Every 10% increase in impervious cover led to an additional 0.80 °C of warming (*p*-value<0.001), while median household income led to an average cooling benefit of 0.349 °C/\$10,000 (*p*-value<0.001).

In the context of these long-term spatial distributions, greenness and temperatures also exhibited temporal variability and trends during the time series (Fig. 3). Between 1985 and 2021 land surface temperature increased $0.13\,^{\circ}$ C/year (p=0.041) and NDVI increased 5.05×10^{-4} per year between 1985 and 2021 (p<0.001). However, the change in NDVI through time was uneven, so that the rate of increase in greenness is different when assessed from different years. Starting in 1992 NDVI increased 6.21×10^{-4} per year (p<0.001), while from 2007 to the end of the time series NDVI increased 0.002 per year (p<0.001). The increase in LST through time was evenly distributed throughout the year, increasing slightly more during the summer months (June–August) at $0.18\,^{\circ}$ C/year (p=0.02) than the winter months (December–February) at $0.15\,^{\circ}$ C/year (p=0.002), although the difference in slopes between seasons was not significant (p=0.17). Partially mitigating this increased heat, vegetative cooling increased $0.08\,^{\circ}$ C/year (p=0.0497). Between 1985 and 2021 urban plants provided an additional $0.96\,^{\circ}$ C/NDVI of cooling. The changes in vegetation and temperature also occurred in the context of a decrease in precipitation of $0.90\,^{\circ}$ C/NDVI of cooling.

Weather plays a significant role in the temporal variability of NDVI and LST at the whole LAUR spatial scale (Fig. 4). The dynamics of urban greenness at the whole city scale was coupled with precipitation and increased 0.007 NDVI per 100 mm of three-months cumulative precipitation (p-value<0.001). Precipitation explained 20% of the temporal variability in NDVI. Urban NDVI was most responsive to precipitation with three months of cumulative rainfall; the fit declined with additional months of rain until nine months

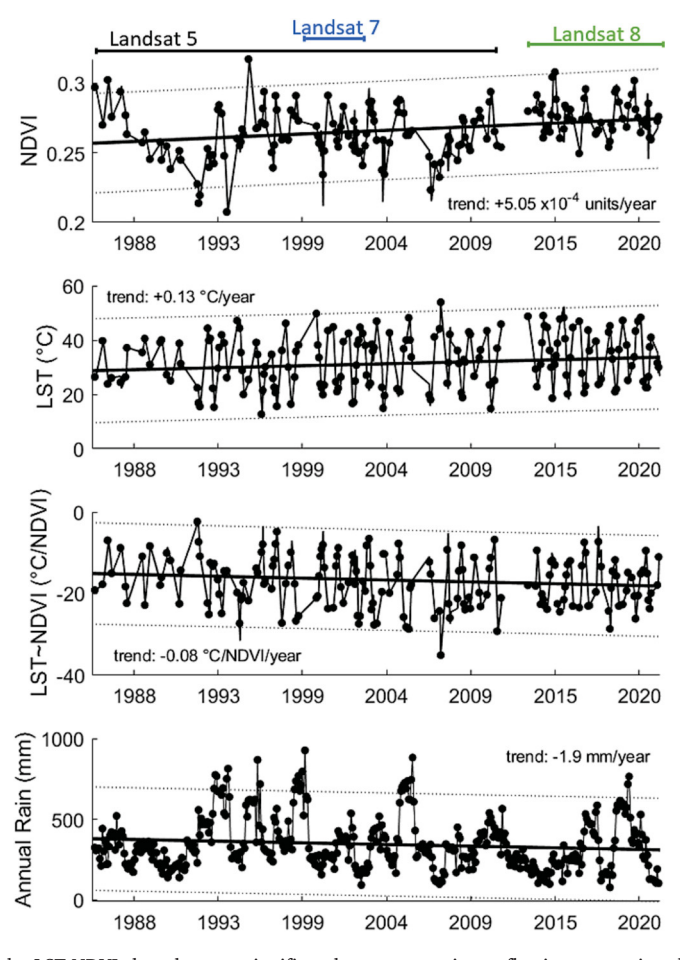


Fig. 3. Between 1985 and 2021 the LST-NDVI slope became significantly more negative, reflecting vegetation that is becoming more efficient at cooling, while urban greenness and temperature both significantly increased through time. A gap in data between December 2011 and March 2013 reflects the period between the end of Landsat 5 and the launch of Landsat 8; Landsat 7 was not used during this period due to the failure of the scan line corrector. These changing NDVI and LST dynamics occurred in the context of increasing aridity, with annual rainfall declining 1.9 mm/year.

of cumulative precipitation when there was no relationship between greenness and precipitation (p-value = 0.47). The weather variables most responsible for the temporal variability in LST were solar radiation and air temperature, which together explained 87% of the variance in LST. Every 1 w/m^2 increase in solar radiation increased LST 0.13 °C, while every 1 °C increase in minimum air temperature increased LST 2.3 °C (p-value<0.001). Solar radiation was the only variable with a partial r^2 of at least 0.05 to significantly modify the temporal variability of vegetative cooling. Vegetative cooling increased with solar radiation at a rate of 0.077 °C/NDVI per 1 w/m^2 , with solar radiation explaining 62% of the temporal variability (p-value<0.001). The temporal variability of NDVI, LST, and vegetative cooling was substantially influenced by the weather, highlighting the key role of weather in shaping urban greenness and temperature dynamics over time.

The temporal trends of greenness and temperature exhibited wide spatial variability in their rates of change within the LAUR (Fig. 5). At both the pixel and census tract scales the median increase in LST was $0.16\,^{\circ}$ C/year with a standard deviation of $0.03\,^{\circ}$ C/year at the pixel scale and of $0.02\,^{\circ}$ C/year at the census tract scale. No pixels exhibited cooling. Pixels at the 5th percentile warmed $0.13\,^{\circ}$ C/year, while pixels at the 95th percentile warmed $0.20\,^{\circ}$ C/year. Aggregated to the census tract scale, only six census tracts warmed $0.20\,^{\circ}$ C/year while only one census tract warmed $0.10\,^{\circ}$ C/year. The median increase in NDVI was $0.10\,^{\circ}$ C/year at the pixel scale with a standard deviation of 0.003, while at the census tract scale, the median increase in NDVI was $0.10\,^{\circ}$ C/year with a standard deviation of 0.003, while at the census tract scale, the median increase in NDVI was $0.10\,^{\circ}$ C/year with a standard deviation of $0.003\,^{\circ}$ C/year

3.2. Variability in the NDVI and LST trends

The per-pixel changes through time in NDVI and LST, when aggregated to the census-tract scale, were most strongly influenced by 2010 per-capita income, while the change in LST was also strongly responsive to the change through time in NDVI (Fig. 6). Every \$10,000 increase in per-capita income increased the NDVI trend 1.32×10^{-4} per year (*p*-value<0.001) while the same increase in income reduced the LST trend by 0.015 °C/year (*p*-value<0.001). The change in greenness had a large effect on the change in

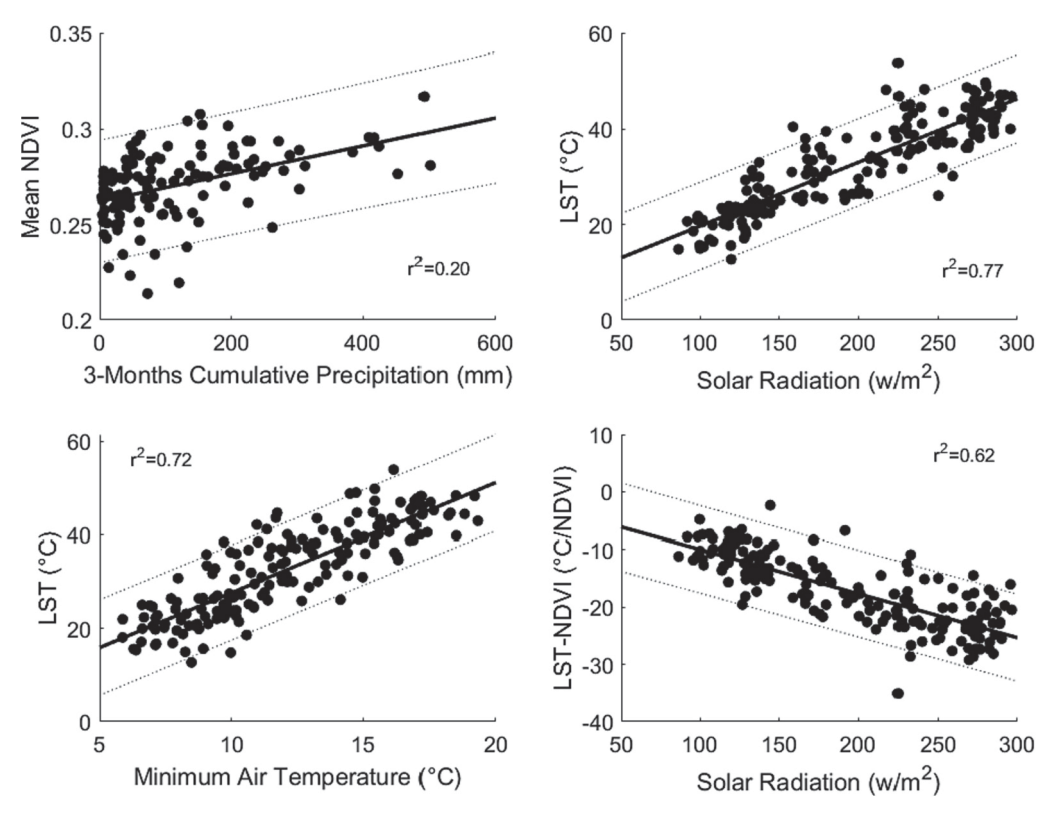


Fig. 4. Urban NDVI, LST, and vegetative cooling responded to changes in the weather; each dot represents a mean monthly value. Despite the LAUR being heavily irrigated, NDVI was still coupled with precipitation with this relationship strongest at a 3-month lag. Solar radiation and air temperature jointly explained 87% of the temporal variability in LST, while vegetative cooling increased with solar radiation.

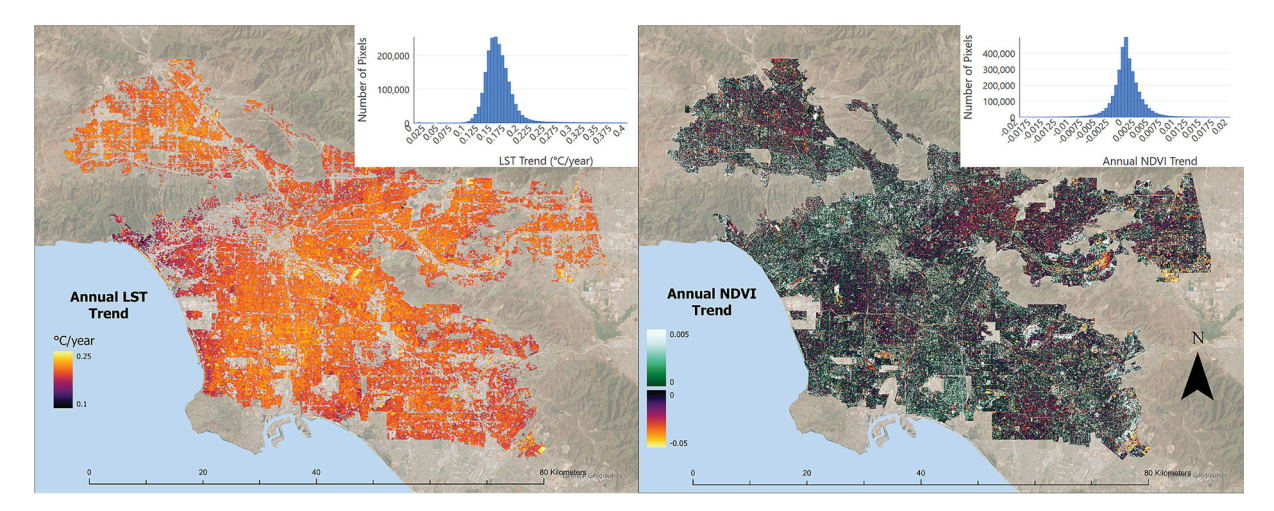


Fig. 5. Between 1985 and 2021 the LAUR warmed everywhere but unevenly; no pixel got significantly cooler. Some regions (in orange and yellow) warmed much faster than the $0.16\,^{\circ}$ C/year per-pixel average. The only region in the lowest tier of cooling ($\leq 0.1\,^{\circ}$ C/year) was along the coast. The regions that got the hottest through time were also spatially related to regions that lost the most greenness. Missing pixels represent regions where the temporal regression was not significant ($p \geq 0.05$). (For interpretation of the references to color in this figure legend, the reader is referred to the web version of this article.)

temperature; every 0.01 NDVI/year increase in greenness was associated with less warming of 0.12 $^{\circ}$ C/year (p < 0.001). We also tested physiographic variables to explain the NDVI and LST trends. Impervious cover had a weak effect on increasing LST, while the distance from the coast had the same effect size on decreasing NDVI. Per-capita income and distance from the coast explain 19% of the spatial variability in the NDVI trend, while per-capita income, impervious cover, and the NDVI trend explain 39% of the spatial variability in the LST trend.

3.3. The NDVI and LST drought response

The effect of drought on NDVI and LST temperature trends was spatially variable (Fig. 7). We assessed the drought response at SPEI-6, as this was the SPEI aggregation that led to the largest change in both NDVI and LST. During drought NDVI decreased on average 0.023, while LST increased 4.41 °C. Vegetative cooling increased 0.08 °C/NDVI during drought. Regions that saw the largest decrease in NDVI (a loss of NDVI of \geq 0.09) visually overlap large urban parks and hilly terrain, however, we did not include fine-scale variability in land cover in our dataset to test this explicitly. Surprisingly, our results indicate that NDVI increased during drought in a minority (13%) of pixels. Aggregated to the census tract scale, no tracts greened during drought. In contrast, the LST drought response exhibited a clear coast-to-inland gradient. During drought inland regions warmed \sim 8 °C, whereas regions right on the coast warmed \sim 2–3 °C. The benefit of the coast in moderating drought temperatures dissipated approximately 5–10 km from the coast. The consistent decrease in greenness and increase in temperature during drought indicates that NDVI and LST may be directly associated

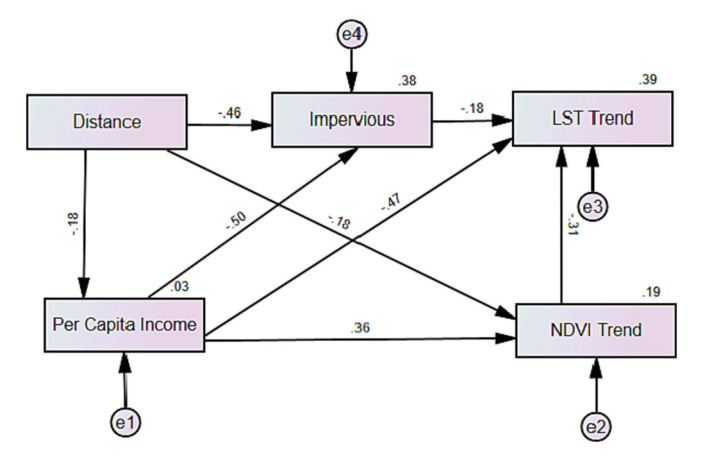


Fig. 6. The change through time of temperature and greenness was best explained by variability in income, as well as in impervious cover and distance from the coast. The wealthiest urban regions saw the slowest rate of warming as well as the greatest increase in greenness. The increase in temperature also increased the slowest in census tracts that saw the most greening.

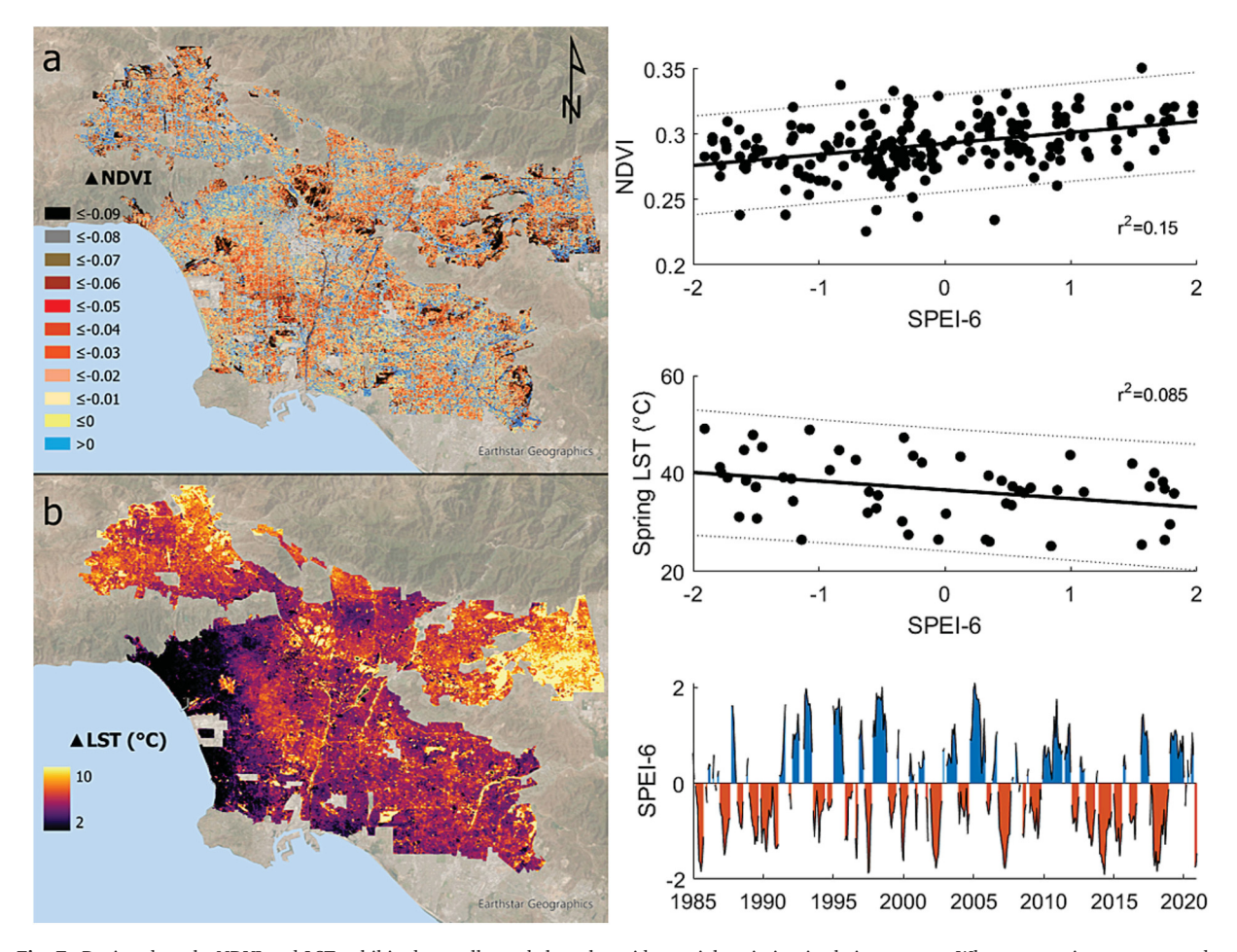


Fig. 7. During drought NDVI and LST exhibited overall trends but also wide spatial variation in their response. When comparing wet versus dry periods at SPEI-6, NDVI decreased on average 0.023, and LST increased on average 4.41 °C. The NDVI response was more spatially heterogeneous, while the LST response exhibited a clear coastal to inland gradient. When regressing all days in the time series against SPEI-6, only NDVI had a significant relationship, increasing by 0.004 with every 0.5 unit increase in SPEI-6. In contrast, the relationship between LST and SPEI-6 was seasonally dependent, with the greatest declines in LST in response to a positive water balance occurring in the spring.

with SPEI. Testing this directly, across all dates NDVI increased 0.007 per unit increase in SPEI-6 (*p*-value<0.001), representing an increase in greenness with a more positive water balance. There was no relationship between SPEI-6 and LST across all dates, however, the relationship between SPEI and LST was seasonally dependent. In the spring (March–June), LST decreased 0.88 °C with every 0.5 unit increase in SPEI. There was no change through time in the severity or frequency of drought at SPEI-6, although drought at interannual SPEI aggregations was becoming more severe and more frequent. Similarly, greenness was responsive to changes in SPEI with greenness increasing during periods of more positive water balance, showcasing the sensitivity of urban vegetation to climatological water availability.

We sought to explain the spatial variability in NDVI and LST during drought at SPEI-6 (Fig. 8). Using multiple regression, we identified all variables explaining the change in NDVI and LST which had a partial r^2 of at least 0.05. The change in NDVI during drought was only influenced by impervious cover ($r^2=0.35$, p-value<0.001), where every 10% decrease in impervious cover led to a greater loss in NDVI of 0.004. As drought predominately led to a decline in NDVI, greater impervious cover led to smaller losses in greenness. The change in LST during drought was more readily explained than that of NDVI. The increase in LST during drought was greatest in regions that lost NDVI ($r^2=0.24$, p-value<0.001) and which were further inland ($r^2=0.44$, p-value<0.001). These two variables explained 61% of the variance in the change in LST during drought. The change in NDVI during drought had an effect 74% larger on the change in LST than that of distance from the coast despite the distance from the coast having a larger effect in univariate regression. LST increased 0.05 °C/km distance from the coast (p-value<0.001) and 0.29 °C per 0.01 loss in NDVI (p-value<0.001). The large spatial and temporal variability in the change in NDVI and LST through time and during drought may have socio-economic and racial consequences.

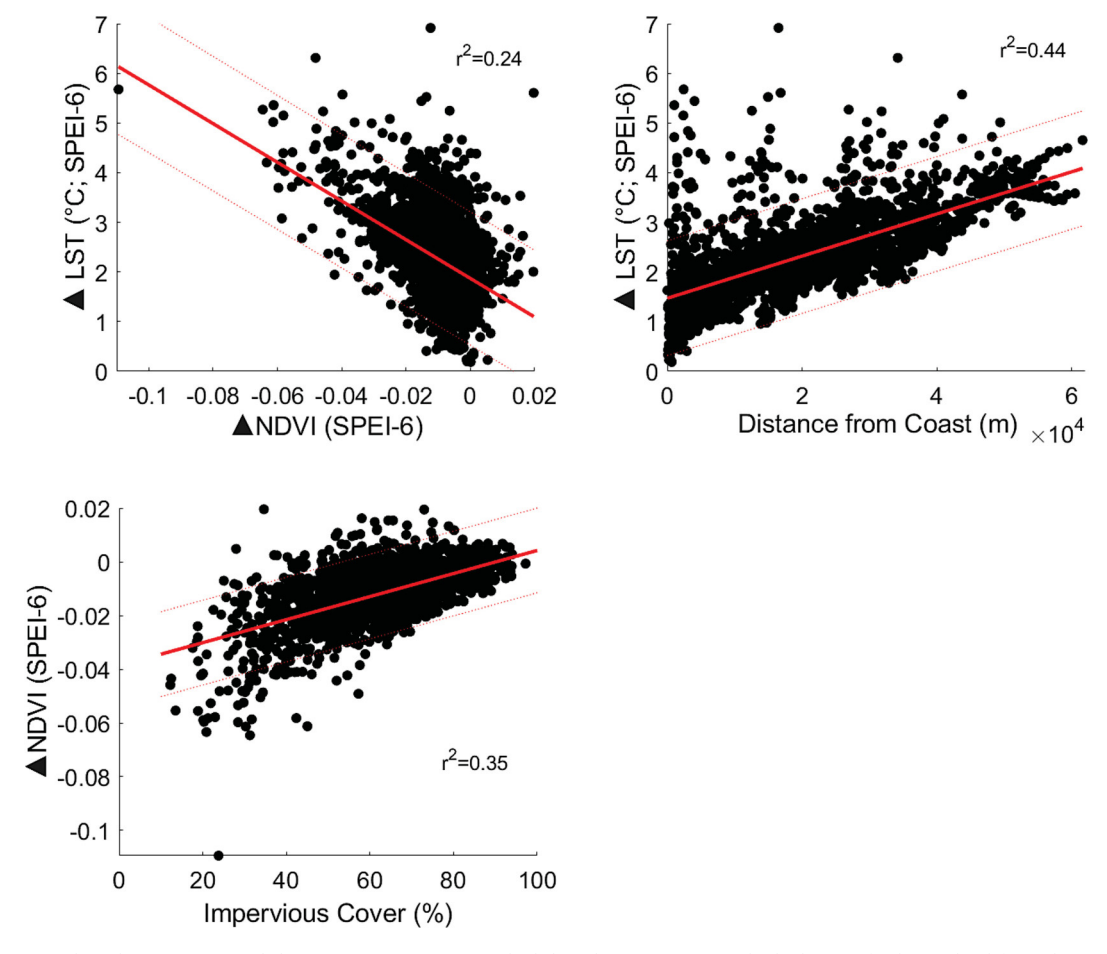


Fig. 8. During drought, LST increased the most in census tracts which lost the most NDVI and which were furthest inland from the coast. From multiple regression, these two variables explained 61% of the variability in the LST drought response. Impervious cover was the only variable identified from multiple regression to modify the NDVI drought response. Greater impervious cover was associated with less change in NDVI during drought, where each point represents one census tract.

3.4. The luxury effect becomes weaker through time and stronger during drought

We found that income had a significantly lower effect on greenness (p-value<0.001) and temperature (p-value<0.001) in 2020 than it did in 1990 (Fig. 9). In 1990, every \$10,000 increase in median household income provided 0.4 °C of cooling and an increase of 0.0202 NDVI. In 2020, the same increase in income provided 0.29 °C of cooling and a 0.0119 increase in NDVI. Income became weaker as a mediator of LST by 0.1 $^{\circ}$ C/\$10,000 (p-value<0.001), an effect 58% as strong in 2020 as it was in 1990, while the effect of income on NDVI declined by 0.008 NDVI/\$10,000 (p-value<0.001), an effect 74% as strong in 2020 as it was in 1990. The decline in the effect of income is concomitant with an increase in the effect of impervious cover on increasing temperature and decreasing greenness. In 2020 every 10% increase in impervious cover led to an additional 0.15 $^{\circ}$ C of warming compared to 1990 (a 24% increase from 0.61 $^{\circ}$ C to $0.76\,^{\circ}$ C; p-value<0.001) and an additional loss of 0.007 NDVI (a 20% decrease from -0.0034 to -0.0042 NDVI; p-value<0.001). In contrast to the weakening of the effect of income through time, the income effect became stronger for LST but not for NDVI during drought (Fig. 10). At an intra-annual scale with SPEI aggregations up to SPEI-10, the effect of income increased, on average, 0.071 °C/ \$10,000 (p-value < 0.001) during dry periods. Notably, droughts of longer duration were associated with increasingly stronger relationships between income and temperature, up until SPEI-11 when the luxury effect became weaker during drought. However, this increase in the effect of income on cooling was not necessarily associated with cooler temperatures at the whole-city scale. Vegetative cooling increased during drought at short timescales (SPEI-2 through SPEI-5) on average 0.99 °C/NDVI (p-value<0.001), while for longer term drought (at SPEI-7 through SPEI-12) vegetative cooling decreased during drought by 1.15 °C/NDVI (p-value<0.001) despite an average increase in the effect of income on cooling of 0.064 °C/\$10,000 between SPEI-7 and SPEI-10 (p-value<0.001). Income-NDVI did not change between wet (SPEI>+1) and dry periods (SPEI<-1), but income-LST became stronger during dry periods. The decline in the effect of income as a mediator of NDVI and LST may have important equity-based consequences.

The non-stationarity of the socio-economic relationships mediating urban greenness and temperatures was also associated with increasingly marginalized minority populations. Throughout the time series, areas with higher Hispanic populations were consistently

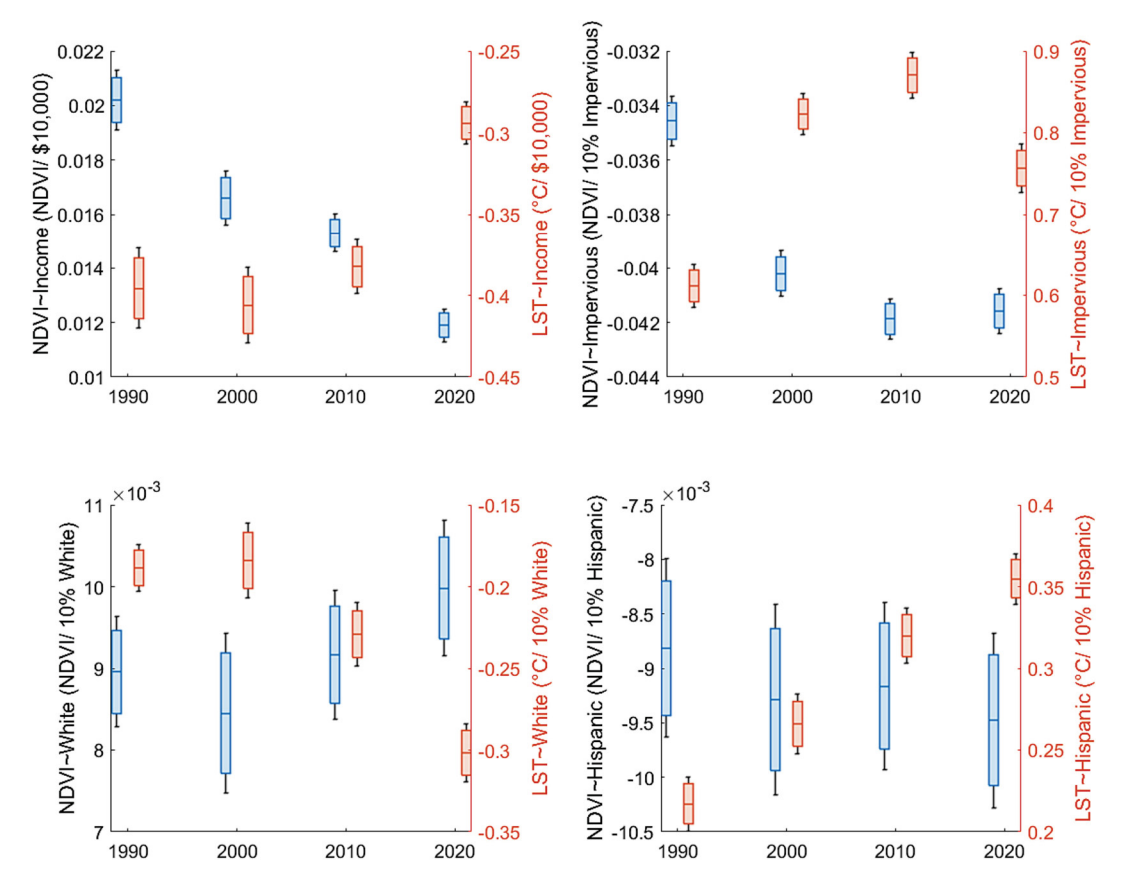


Fig. 9. Between 1990 and 2020 the effect of income on increasing greenness and decreasing temperatures significantly declined. As the LAUR has gotten hotter the luxury effect has gotten weaker. In 1990 \$10,000 of income led to a 0.4 °C decrease in LST, whereas in 2020 the same increase in income led to a 0.29 °C decrease. In conjunction with the weakening of the luxury effect, the effect of impervious cover on decreasing greenness and increasing temperatures increased through time. These differences were race specific. Despite the weakening effect of income, Hispanic communities experienced greater heat through time while White communities did not. Blue boxplots refer to the left y-axis, representing the relationship between NDVI and either income, impervious cover, percent White population, or percent Hispanic population. Orange boxplots refer to the right y-axis and represent the relationship between LST and the same variables. (For interpretation of the references to color in this figure legend, the reader is referred to the web version of this article.)

found to have increased LST and reduced greenness. Over time, the association between Hispanic-dominated neighborhoods and increased LST significantly strengthened. Compared to 1990, by 2020 LST warming associated with Hispanic-dominated neighborhoods increased 63%; in 1990 every 10% increase in a census tract's Hispanic population increased LST 0.22 °C while the same increase in Hispanic populations increased LST 0.35 °C in 2020. Likewise, the association between Hispanic-dominated neighborhoods and reduced greenness strengthened through time, although this change was not significant. Compared to 1990, by 2020 every 10% increase in a census tract's Hispanic population led to an additional 8% loss in greenness, but this additional decline in greenness was not significant. White-dominated neighborhoods did not experience similar trajectories. In 1990 every 10% increase in the census tract White population led to an increase in NDVI of 0.01 and a decrease in LST of 0.19 °C. In 2020 the same increase in the White population led to the same 0.01 increase in NDVI and a significant 58% increase in cooling to 0.30 °C. Whereas the experience of Hispanic populations with regards to greenness and temperature is unchanged and significantly worse, respectively, the experience of White populations with regards to greenness and temperature is unchanged and significantly better, respectively. This dichotomy is not reflective of the race-specific changes in the effect of income (Fig. 11); the effect of income on both NDVI and LST declined proportionally similar amounts between White and Hispanic populations. Between 2000 (the first year we had race-specific income data) and 2020, the effect of income declined across White, Hispanic, Black, and Asian communities, with the decline most strongly driven by a decline in the effectiveness of income in White and Hispanic communities. The effect of income was always greatest in White populations and always lowest in Black and Asian populations. In 2000, income in White communities provided 2.42× as much greening and 2.68× as much cooling as the same income in Black communities, declining to an effect 2.12× and 2.31× greater by the 2020 census.

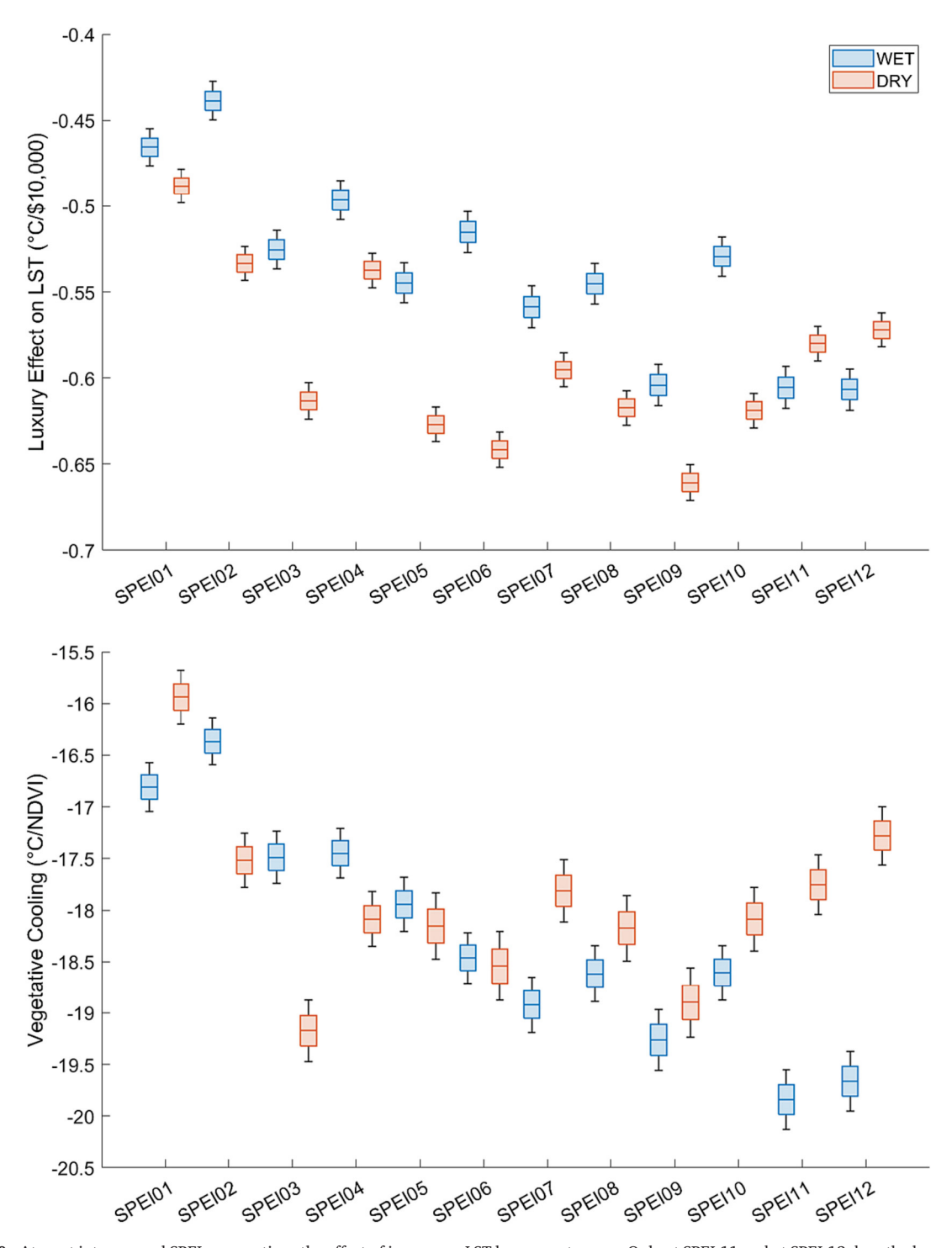


Fig. 10. At most intra-annual SPEI aggregations the effect of income on LST becomes stronger. Only at SPEI-11 and at SPEI-12 does the luxury effect on temperature become weaker during drought. This increase in the luxury effect is not necessarily reflected in increased vegetative cooling; drought may slightly increase vegetative cooling for sub-6-month SPEI aggregations, but from SPEI-7 and up vegetative cooling declines during drought.

4. Discussion

In the Los Angeles urban region over the past 36 years, urban greenness, land surface temperatures, and the cooling effectiveness of vegetation have all increased. These trajectories were related to changes in weather patterns, exhibited extensive spatial heterogeneity

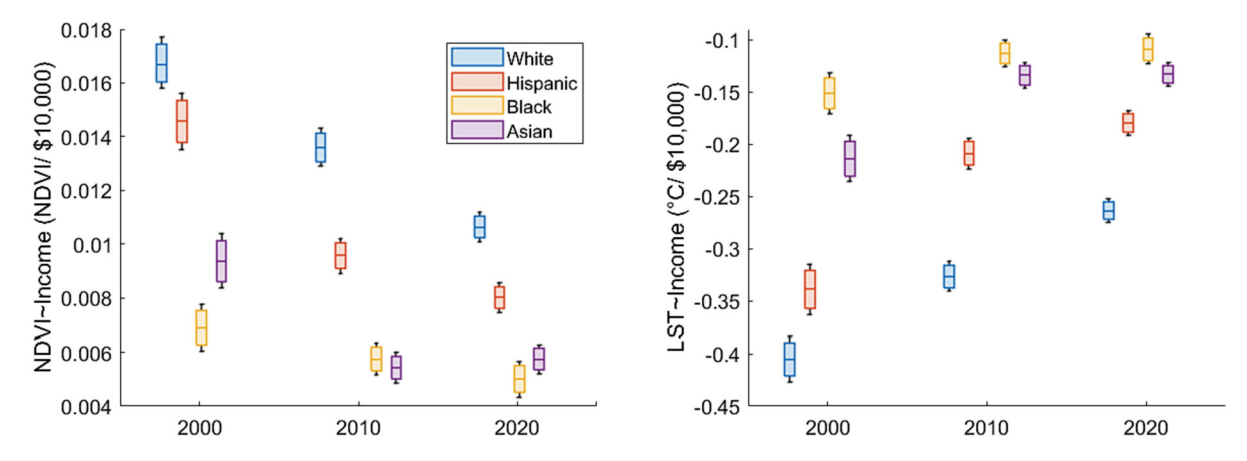


Fig. 11. The decrease in the luxury effect was primarily due to a reduction in the relationships between income and both LST and NDVI in white communities, with similar declines in Hispanic and Asian communities. The influence of income was not uniform across races. As per the 2000 census data, the same amount of income in white communities led to 2.68 times as much cooling and 2.42 times as much greening compared to Asian and black communities. Over time, the impact of income on cooling and greening has become more equitable across races due to city-wide declines in the effectiveness of income.

associated with physiographic and demographic distributions, and were associated with changing patterns of equity in access to greenspace and heat risks. Droughts were consistently associated with increased temperature and decreased greenness. However, land cover distributions moderated the drought response, consistent with our hypothesis on the importance of physiography. The temporal increases in LST and NDVI are consistent with climate changes and tree-planting campaigns. The increase in LST through time was at least partially mitigated by an increase in vegetative cooling. The modification of the NDVI and LST trends in response to income, distance from the coast, and impervious cover supports our hypothesis about the importance of water availability. At the monthly scale, weather explains temporal variability in NDVI, LST, and vegetative cooling, and the spatial variability across the urban extent is explained by land cover and income alone. These results suggest the capacity to manage the dynamics of NDVI and LST has declined through time with the decline of the luxury effect. Despite the decline in the effectiveness of income, the changing urban dynamics led to the increasing marginalization of predominantly Hispanic communities but an improvement in conditions for predominantly White communities. Overall, our results show the multidecadal dynamics of NDVI, LST, and vegetative cooling are multifactorial and have important race-based equity implications.

From 1985 to 2021, NDVI, LST, and vegetative cooling increased in the context of decreasing annual precipitation (Fig. 3). Vegetative cooling (°C LST/NDVI), standardized on a per-unit NDVI basis, suggests that the urban vegetation within LAUR is becoming more effective over time. Increased cooling may be due to increased transpiration from warming-induced evaporative demand (Kirschbaum, 2004; Drake et al., 2018). The multidecadal increase in greenness and temperature are consistent with tree planting campaigns and climate change, respectively. The average city-wide increase in LST of 0.13 °C/year is consistent with other cities such as Atlanta, USA (Fu and Weng, 2016), Ahmedabad, India (Siddiqui et al., 2021), and Marseille, France (Polydoros et al., 2018). Temporal variability in NDVI, LST, and vegetative cooling was unaffected by anthropogenic variables, as variables such as income and land cover may minimally change on a month-to-month basis. NDVI, LST, and vegetative cooling increased through time; we sought to explain the spatial variability in these trends.

The dynamics of NDVI, LST, and vegetative cooling were well correlated with the weather (Fig. 4). Precipitation, temperature, and solar radiation were key drivers of monthly temporal variability. Despite the LAUR being a heavily irrigated semi-arid city, NDVI was sensitive to cumulative rainfall, increasing the most in response to three months of cumulative precipitation. The overall sensitivity of LAUR urban greenness to precipitation contrasts with the finding from Phoenix, AZ where urbanization completely decoupled urban greenness from precipitation (Buyantuyev and Wu, 2012). However, Phoenix is in a desert climate that receives 57% of the annual rainfall of the LAUR, a semi-arid city. The finding that urbanization does not decouple greenness from precipitation in a Mediterranean city like the LAUR is consistent with Jenerette et al. (2013) and suggests that the decoupling of urban greenness from precipitation occurs along a gradient of precipitation where decoupling occurs only in the most arid cities. Further, during the 2011–2016 California megadrought, the most severe in over a millennium (Griffin and Anchukaitis, 2014), we observed a decrease in NDVI in the LAUR, consistent with findings from another California city where urban greenness decreased despite little change in irrigation (Quesnel et al., 2019). This hint of an underlying water deficit despite anthropogenic input (Bijoor et al., 2012) suggests an urban water deficit hypothesis, where neighborhood greenness and temperature are modified by the difference between irrigation and evaporative demand yet where anthropogenic inputs do not fully satisfy plant water demands. In contrast to the importance of weather for temporal variability, tree canopy cover and income were the only determinants of the spatial variability of NDVI and LST (Supplemental Figs. 1 & 2); in the LAUR anthropogenic drivers overrode any effect natural drivers have on the spatial variability of NDVI and LST. The preeminence of anthropogenic drivers may be related to the composition of the LAUR's urban forest. This sensitivity of the spatial variability of NDVI and LST to anthropogenic factors is suggestive that NDVI and LST are sensitive to water availability and water demand, supporting our urban water deficit hypothesis. We suspect the dominance of anthropogenic variables in explaining spatial

variability may be particularly important for the LAUR as it exists in a semi-arid environment, making the dynamics of urban greenness and temperature more sensitive to urban tree cover and irrigation. The spatial and temporal variability of NDVI, LST, and vegetative cooling were dependent on water availability and water demand.

Compared to hotter and drier inland semi-arid cities, the LAUR experiences a milder thermal environment due to its coastal location which moderates temperatures via sea breezes. For example, the daytime land surface temperature in the LAUR averaged 35 °C annually, while inland semi-arid cities like Jaipur, India experienced much higher average summer land surface temperatures exceeding 50 °C (Shahfahad et al., 2023). The relatively mild summer temperatures in coastal Mediterranean climates like Los Angeles allow urban vegetation to thrive and provide substantial local cooling through evapotranspiration and shading, though in a climatically similar coastal Mediterranean city vegetative cooling was greatest in the spring and summer (Dronova et al., 2018). For instance, Los Angeles parks generate 4.73 °C of local cooling with a cooling distance of 165 m (Gao et al., 2022), compared to summertime cooling from parks in more inland semi-arid cities such as Tehran of 0.8 °C for up to 68 m (Jamali et al., 2021). In contrast, (Li et al., 2015) found that in the inland semi-arid city of Beijing, differences in latent heat fluxes between urban and rural areas lead to heat wave intensification of urban heat islands, constraining the cooling capacity of vegetation. Overall, the relatively mild climate of the LAUR enables urban greenery to more effectively mitigate urban heat compared to drier and hotter inland semi-arid cities. This greater mitigation capacity is reflected in the long-term increasing trend in vegetative cooling in the LAUR.

At the pixel scale there was wide spatial variability in the NDVI and LST trends (Fig. 5). While trends of NDVI and LST have been conducted at a city-wide scale (Voogt and Oke, 2003; Imhoff et al., 2010; Ren et al., 2021; Yang et al., 2021), several studies have shown substantial heterogeneity of the intraurban environment (Liu et al., 2021; Jombo et al., 2022; Lemoine-Rodriguez et al., 2022; Purio et al., 2022). In the LAUR, temperature increased the most in low-income communities that lost greenness, suggesting that the dynamics of NDVI and LST have been inequitably distributed and that inequity is increasing through time. Spatial inequities in urban heat (Reid et al., 2009; Harlan et al., 2013) and greenness (Boone et al., 2009; Jennings et al., 2012) are therefore being propagated through time in the LAUR. The multidecadal change in greenness and temperature was spatially variable, and via income was partially associated with anthropogenic inputs of water (Fig. 6). To explain this variability we looked at drought, being a natural extreme of both water availability and, via aridity, water demand, as a possible determinant of the dynamics of urban NDVI, LST, and vegetative cooling.

The urban water deficit hypothesis suggests that, during drought, changes in NDVI, LST, or vegetative cooling would be closely associated with variables that modify water availability or demand (Fig. 7). We found partial support for this hypothesis. Greenness decreased the most in regions with low impervious cover, which was the only variable we identified to modify this relationship (Fig. 8). The increase in greenness in a minority of pixels at SPEI-06 may also be due to impervious cover, as many, but not all, of the pixels which greened overlap with impervious surfaces like roads and business centers. We interpret the importance of impervious cover in determining the change in NDVI during drought to suggest two things: first, that census tracts with greater open space (e.g., large urban parks), may have vegetation that is less actively managed than vegetation in highly impervious landscapes (e.g., street trees or vegetation at a residential property). Second, the decline in greenness during drought with increasing pervious cover suggests that drought negatively affects all vegetation and that in regions with a greater potential amount of vegetated cover, via less impervious cover, more greenness can potentially be lost during drought. Increasing distance from the coast is associated with increased evaporative demand (Vasey et al., 2014; Tayyebi and Jenerette, 2016), supporting our urban water deficit hypothesis that the change in LST would be greater in regions with a larger difference between water availability and water demand (Fig. 8). In this context, water availability is the total amount of water available for plants, whether from irrigation or rain. Water demand refers to the water requirements of plants, and here would be driven by atmospheric aridity and temperature. Within a few kilometers of the coast the maritime environment, which includes cooler, cloudier conditions, appears to have mitigated the increase in temperature associated with drought. The regions furthest inland, in contrast, warmed the most during drought; this was driven by a decrease in vegetative greenness which subsequently decreased vegetative cooling. The loss of greenness was the most important variable to increase temperature during drought, consistent with our finding of the strong relationship between temperature and greenness over multidecadal periods. Although the coast-to-inland gradient for the change in temperature during drought was more pronounced from west to east than from south to north, this likely occurred because the minimal Landsat imagery on the coast for the southern region of the study area was unable to capture the coastal phenomena, which is only present within a few kilometers of the coast. Finally, drought increased vegetative cooling, suggesting that increased aridity increased transpiration (Fig. 10). Contrary to Allen et al. (2021) who observed a decrease in urban cooling capacity during drought, our study found drought to increase vegetative cooling; this discrepancy likely stems from the differing conceptualizations of 'drought' across studies, underlining the necessity to interpret drought effects on urban greenness and temperature in the context of their specific definitions and parameters (Slette et al., 2019). Drought led to consistent decreases in greenness and temperature increases that were able to be explained via potential plantable space and the urban water deficit hypothesis. The resulting spatial heterogeneity of the dynamics of NDVI and LST appears to have important equity

As a consequence of changes in greenness and heat, our results suggest the luxury effect, an important driver of the spatial heterogeneity of urban greenness and temperature, is becoming weaker through time (Fig. 9) but stronger during drought (Fig. 10). Between 1990 and 2020 the effect of income on temperature declined 41% while the effect on greenness declined 28%. The decline of the luxury effect through time despite the LAUR's increasing aridity is counter to our hypothesis that the effect of income on mediating temperature and greenness would increase with greater aridity. The non-stationarity of income in its relationship with NDVI and LST underscores the dynamic and complex influence of socioeconomic factors on urban ecological patterns (Romolini et al., 2013; Fan et al., 2019), warranting further investigation into the mechanisms behind this temporal variability. The luxury effect may have declined due to wealthy residents actively reducing greenness as they transitioned to drought-tolerant landscaping. Los Angeles and

surrounding communities have been aggressively replacing water-intense landscaping with xeriscaping, a practice known to raise urban temperatures 1.8 °C in arid cities (Dialesandro et al., 2019). In 2014 Los Angeles replaced 9.8 million m² of turfgrass (Pincetl et al., 2019), however, affluent residents may have a greater capacity to install drought-tolerant landscaping (Larson and Brumand, 2014). During drought between SPEI-01 and SPEI-10 the luxury effect increased for income-LST but not for income-NDVI, partially supporting our hypothesis that higher-income neighborhoods use more water during drought. Income, via the luxury effect, may become more important with aridity due to the increased demand for water at a higher VPD (Chamberlain et al., 2020). Higher-income neighborhoods have been associated with more water consumption following droughts (Balling et al., 2008; House-Peters et al., 2010), potentially enhancing the luxury effect during drought. This may explain the strengthening of the luxury effect with droughts of increasing duration up to SPEI-11. However, the increase in the importance of income on mediating urban temperature during drought did not always lead to greater cooling overall. The increase in vegetative cooling during droughts from SPEI-2 to SPEI-5 suggests that existing water reserves and irrigation unrestricted by water limitations served to increase cooling under conditions of greater atmospheric aridity. The trend reversed at SPEI-7 and above, suggesting that for droughts longer than half a year, irrigation restrictions as well as depleted soil water reserves were insufficient to meet vegetative transpiration water demands. This likely also explains the inverted relationship of income with LST at SPEI-11, where the luxury effect becomes weaker during drought. However, the increased importance of income in mediating temperature during drought between SPEI-01 and SPEI-10 suggests that wealthy regions are somewhat insulated from increased temperatures during drought. The changing magnitude of the luxury effect highlights how variables that modify urban greenness and temperature are not stable across time. We found these changing relationships were also dissimilar by race.

The decline in the luxury effect across time is primarily driven by a reduction in the correlation between income in White and Hispanic communities. The decline in the luxury effect was at least partially responsible for the increasing marginalization of Hispanic populations but did not explain the improvement of conditions for White populations. The multidecadal increase in temperature associated with Hispanic census tracts, despite White census tracts being associated with greater cooling through time, points to an increasingly inequitable pattern of urban warming where Hispanic residents are bearing the brunt of rising urban heat compared to historically White areas (Fig. 9). This increasing inequity may be associated with green investment preferentially targeted to wealthy neighborhoods (Locke and Grove, 2014; Shokry et al., 2020), whereas green investment in low-income neighborhoods may lead to gentrification and displacement (Anguelovski et al., 2017; Keenan et al., 2018). The disparity in the experience of White and Hispanic populations in their ability to mediate temperature is not reflective of race-based changes in the luxury effect, which proportionally declined a similar amount between White and Hispanic populations (Fig. 11). The different trajectories of how White and Hispanic communities experience greenness and temperature suggests a mediating variable other than income is rising in importance as the effect of income declines. For instance, communities of color are characterized by greater impervious cover (Fossa et al., 2023), which is known to increase urban heat (Tian et al., 2021; Yang et al., 2021). Further, these decoupled trajectories may be explained by increasing urban wealth; although the effect of income is declining, there is more income over time, and there is more income overall in White communities versus Hispanic ones (Flippen, 2016). Inequitable urban warming linked to racial and socioeconomic disparities in vegetation has been widely documented and poses dangers to public health (Jesdale et al., 2013; Oudin Åström et al., 2013). Communities of color, independent of income, are disproportionately exposed to high urban heat (Benz and Burney, 2021; Hsu et al., 2021) and their negative health effects on morbidity and mortality (Harlan et al., 2014; James et al., 2016; Son et al., 2016; Murage et al., 2020). The observed decline in the luxury effect reflects a narrowing equity gap as the effect of income converges towards a minimum income effectiveness among all races, leading to risk for people already living in hot/unvegetated neighborhoods. The complex relationship between urban temperatures, race, and income poses challenges for urban land managers striving to improve environmental justice for increasingly marginalized minority populations. Addressing greenspace inequity is a key step towards mitigating the intensifying heat impacts experienced by these communities (Jennings et al., 2019; Kephart, 2022).

5. Synthesis / conclusions

The world is warming, urban drought is increasing, and the atmosphere is drying, increasing the importance of understanding how urban ecosystems will respond. Our 36-year longitudinal study of the Los Angeles urban region reveals notable racial inequities: Hispanic communities faced disproportionate warming when compared to their White counterparts. Over the whole LA region, average land surface temperature (LST) increased by 0.13 °C per annum, while the mean NDVI (Normalized Difference Vegetation Index) increased by 0.0009 each year. Interestingly, we observed an increase in vegetative cooling through time of 0.08 °C/year, suggesting urban vegetation became more effective at cooling. Vegetative cooling is strongly related to income; however, we observed a decline of 28% and 41% in the luxury effect for income-NDVI and income-LST relationships, respectively. As cities like Los Angeles grapple with intensifying heat and dryness, urban planners and land managers need better resources to forecast how urban ecosystems will respond. However, the non-stationarity observed in NDVI, LST, and vegetative cooling dynamics suggest that past patterns may not reliably predict future dynamics. However, this study wasn't without its limitations. While the spatial granularity of our Landsat satellite data provided valuable insights into broad urban trends, the resolution might not capture finer neighborhood-level nuances. Employing higher-resolution data and integrated modeling could help elucidate these micro-scale patterns and strengthen the links between environmental factors and social dimensions. Future research could bridge these gaps by employing higher-resolution imagery, collecting in-situ demographic data, and using integrated models that utilize climate, hydrology, social aspects, and land use. The observed increasing marginalization of Hispanic communities compared to White communities emphasizes the importance of environmental justice initiatives; the entrenchment of these spatial inequities through time is likely exhibited in other cities. Recognizing the non-stationarity of urban relationships underscores the necessity for continuous re-evaluation in urban ecological

research, as the dynamics we currently observe may evolve, challenging our existing understanding and management of urban ecosystems.

CRediT authorship contribution statement

Dion Kucera: Writing – original draft, Conceptualization, Formal analysis, Funding acquisition, Investigation. **G. Darrel Jenerette:** Supervision, Writing – review & editing, Funding acquisition.

Declaration of Competing Interest

The authors declare no competing interests relating to employment, funding, honoraria, or otherwise which influenced the results of this paper.

Data availability

Data are publicly archived.

Acknowledgments

We are grateful to Dr. Peter Ibsen for his thoughtful critique and insightful feedback that significantly improved our manuscript. As well, this research was funded by grants EAR–1923150 and CNH-1924288 from the National Science Foundation, and fellowships from the Los Angeles Center for Urban Natural Resources Sustainability and the UCR/NASA Fellowships and Internships in Extremely Large Data Sets (FIELDS).

Appendix A. Supplementary data

Supplementary data to this article can be found online at https://doi.org/10.1016/j.uclim.2023.101743.

References

Abatzoglou, J.T., Dobrowski, S.Z., Parks, S.A., Hegewisch, K.C., 2018. TerraClimate, a high-resolution global dataset of monthly climate and climatic water balance from 1958-2015. Sci. Data 5, 170191.

Allen, M.A., Roberts, D.A., McFadden, J.P., 2021. Reduced urban green cover and daytime cooling capacity during the 2012–2016 California drought. Urban Clim. 36. Anguelovski, I., Connolly, J.J.T., Masip, L., Pearsall, H., 2017. Assessing green gentrification in historically disenfranchised neighborhoods: a longitudinal and spatial analysis of Barcelona. Urban Geogr. 39, 458–491.

Balling, R.C., Gober, P., Jones, N., 2008. Sensitivity of residential water consumption to variations in climate: an intraurban analysis of Phoenix, Arizona. Water Resour. Res. 44.

Banskota, A., Kayastha, N., Falkowski, M.J., Wulder, M.A., Froese, R.E., White, J.C., 2014. Forest monitoring using Landsat time series data: a review. Can. J. Remote. Sens. 40, 362–384.

Barrera, F.D.L., Henriquez, C., Ruiz, V., Inostroza, L., 2019. Urban parks and social inequalities in the access to ecosystem services in Santiago, Chile. IOP Conf. Ser. Mater. Sci. Eng. 471.

Benz, S.A., Burney, J.A., 2021. Widespread race and class disparities in surface urban heat extremes across the United States. Earths Future 9.

Bijoor, N.S., McCarthy, H.R., Zhang, D., Pataki, D.E., 2012. Water sources of urban trees in the Los Angeles metropolitan area. Urban Ecosyst. 15, 195–214. Boone, C.G., Buckley, G.L., Grove, J.M., Sister, C., 2009. Parks and people: an environmental justice inquiry in Baltimore, Maryland. Ann. Assoc. Am. Geogr. 99, 767–787.

Borowik, T., Pettorelli, N., Sönnichsen, L., Jędrzejewska, B., 2013. Normalized difference vegetation index (NDVI) as a predictor of forage availability for ungulates in forest and field habitats. Eur. J. Wildl. Res. 59, 675–682.

Breger, B.S., Eisenman, T.S., Kremer, M.E., Roman, L.A., Martin, D.G., Rogan, J., 2019. Urban tree survival and stewardship in a state-managed planting initiative: a case study in Holyoke, Massachusetts. Urban For. Urban Green. 43.

Broadbent, A.M., Coutts, A.M., Tapper, N.J., Demuzere, M., 2018. The cooling effect of irrigation on urban microclimate during heatwave conditions. Urban Clim. 23, 309–329.

Buyantuyev, A., Wu, J., 2012. Urbanization diversifies land surface phenology in arid environments: interactions among vegetation, climatic variation, and land use pattern in the Phoenix metropolitan region, USA. Landsc. Urban Plan. 105, 149–159.

Buyantuyev, A., Wu, J., Gries, C., 2007. Estimating vegetation cover in an urban environment based on Landsat ETM+ imagery: a case study in Phoenix, USA. Int. J. Remote Sens. 28, 269–291.

Carlson, T.N., Ripley, D.A., 1997. On the relation between NDVI, fractional vegetation cover, and leaf area index. Remote Sens. Environ. 62, 241–252.

Casey, J.A., James, P., Cushing, L., Jesdale, B.M., Morello-Frosch, R., 2017. Race, ethnicity, income concentration and 10-year change in urban greenness in the United States. Int. J. Environ. Res. Public Health 14.

Chamberlain, D., Reynolds, C., Amar, A., Henry, D., Caprio, E., Batáry, P., McGill, B., 2020. Wealth, water and wildlife: landscape aridity intensifies the urban luxury effect. Glob. Ecol. Biogeogr. 29, 1595–1605.

Chen, X., Zhao, P., Hu, Y., Ouyang, L., Zhu, L., Ni, G., 2019. Canopy transpiration and its cooling effect of three urban tree species in a subtropical city- Guangzhou, China. Urban For. Urban Green. 43.

Cheng, X., Liu, Y., Dong, J., Corcoran, J., Peng, J., 2023. Opposite climate impacts on urban green spaces' cooling efficiency around their coverage change thresholds in major African cities. Sustain. Cities Soc. 88.

Clarke, P., Morenoff, J., Debbink, M., Golberstein, E., Elliott, M.R., Lantz, P.M., 2014. Cumulative exposure to neighborhood context: consequences for health transitions over the adult life course. Res. Aging 36, 115–142.

Cook, M., Schott, J., Mandel, J., Raqueno, N., 2014. Development of an operational calibration methodology for the Landsat thermal data archive and initial testing of the atmospheric compensation component of a land surface temperature (LST) product from the archive. Remote Sens. 6, 11244–11266.

- Corral-Verdugo, V.C., Bechtel, R.B., Fraijo-Sing, B., 2003. Environmental beliefs and water conservation: an empirical study. J. Environ. Psychol. 23, 247-257.
- Coseo, P., Larsen, L., 2014. How factors of land use/land cover, building configuration, and adjacent heat sources and sinks explain urban heat islands in Chicago. Landsc. Urban Plan. 125, 117–129.
- Cunha, A.P.M., Alvalá, R.C., Nobre, C.A., Carvalho, M.A., 2015. Monitoring vegetative drought dynamics in the Brazilian semiarid region. Agric. For. Meteorol. 214-215. 494-505.
- Dialesandro, J.M., Wheeler, S.M., Abunnasr, Y., 2019. Urban heat island behaviors in dryland regions. Environ. Res. Commun. 1.
- Drake, J.E., Tjoelker, M.G., Varhammar, A., Medlyn, B.E., Reich, P.B., Leigh, A., Pfautsch, S., Blackman, C.J., Lopez, R., Aspinwall, M.J., Crous, K.Y., Duursma, R.A., Kumarathunge, D., De Kauwe, M.G., Jiang, M., Nicotra, A.B., Tissue, D.T., Choat, B., Atkin, O.K., Barton, C.V.M., 2018. Trees tolerate an extreme heatwave via sustained transpirational cooling and increased leaf thermal tolerance. Glob. Chang. Biol. 24, 2390–2402.
- Dronova, I., Friedman, M., McRae, I., Kong, F., Yin, H., 2018. Spatio-temporal non-uniformity of urban park greenness and thermal characteristics in a semi-arid region. Urban For. Urban Green. 34, 44–54.
- Dwyer, J.L., Roy, D.P., Sauer, B., Jenkerson, C.B., Zhang, H.K., Lymburner, L., 2018. Analysis ready data: enabling analysis of the Landsat archive. Remote Sens. 10. Eisenman, T.S., Flanders, T., Harper, R.W., Hauer, R.J., Lieberknecht, K., 2021. Traits of a bloom: a nationwide survey of U.S. urban tree planting initiatives (TPIs). Urban For. Urban Green. 61.
- Elkhrachy, I., 2018. Vertical accuracy assessment for SRTM and ASTER Digital Elevation Models: A case study of Najran city, Saudi Arabia. Ain Shams Eng. J. 9, 1807–1817.
- Esau, I., Miles, V.V., Davy, R., Miles, M.W., Kurchatova, A., 2016. Trends in normalized difference vegetation index (NDVI) associated with urban development in northern West Siberia. Atmos. Chem. Phys. 16, 9563–9577.
- Fan, C., Johnston, M., Darling, L., Scott, L., Liao, F.H., 2019. Land use and socio-economic determinants of urban forest structure and diversity. Landsc. Urban Plan. 181, 10–21.
- Feng, W., Lu, H., Yao, T., Yu, Q., 2020. Drought characteristics and its elevation dependence in the Qinghai-Tibet plateau during the last half-century. Sci. Rep. 10, 14323.
- Flippen, C.A., 2016. Racial and ethnic inequality in homeownership and housing equity. Sociol. Q. 42, 121-149.
- Fossa, A.J., Zelner, J., Bergmans, R., Zivin, K., Adar, S.D., 2023. Sociodemographic correlates of greenness within public parks in three U.S. cities. Wellbeing Space Soc. 5.
- Fu, P., Weng, Q., 2016. A time series analysis of urbanization induced land use and land cover change and its impact on land surface temperature with Landsat imagery. Remote Sens. Environ. 175, 205–214.
- Gao, K., Santamouris, M., Feng, J., 2020. On the cooling potential of irrigation to mitigate urban heat island. Sci. Total Environ. 740, 139754.
- Gao, Z., Zaitchik, B.F., Hou, Y., Chen, W., 2022. Toward park design optimization to mitigate the urban heat island: assessment of the cooling effect in five U.S. cities. Sustain. Cities Soc. 81.
- Garrison, J.D., 2017. Seeing the park for the trees: New York's "million trees" campaign vs. the deep roots of environmental inequality. Environ. Plan. B Urban Anal. City Sci. 46, 914–930.
- Garrison, J.D., 2018. Environmental justice in theory and practice: measuring the equity outcomes of Los Angeles and New York's "million trees" campaigns. J. Plan. Educ. Res. 41, 6–17.
- Gillespie, T.W., de Goede, J., Aguilar, L., Jenerette, G.D., Fricker, G.A., Avolio, M.L., Pincetl, S., Johnston, T., Clarke, L.W., Pataki, D.E., 2016. Predicting tree species richness in urban forests. Urban Ecosyst. 20, 839–849.
- Gorelick, N., Hancher, M., Dixon, M., Ilyushchenko, S., Thau, D., Moore, R., 2017. Google earth engine: planetary-scale geospatial analysis for everyone. Remote Sens. Environ. 202, 18–27.
- Griffin, D., Anchukaitis, K.J., 2014. How unusual is the 2012-2014 California drought? Geophys. Res. Lett. 41, 9017-9023.
- Grossiord, C., Buckley, T.N., Cernusak, L.A., Novick, K.A., Poulter, B., Siegwolf, R.T.W., Sperry, J.S., McDowell, N.G., 2020. Plant responses to rising vapor pressure deficit. New Phytol. 226, 1550–1566.
- Harlan, S.L., Brazel, A.J., Prashad, L., Stefanov, W.L., Larsen, L., 2006. Neighborhood microclimates and vulnerability to heat stress. Soc. Sci. Med. 63, 2847–2863. Harlan, S.L., Declet-Barreto, J.H., Stefanov, W.L., Petitti, D.B., 2013. Neighborhood effects on heat deaths: social and environmental predictors of vulnerability in Maricona County, Arizona, Environ. Health Perspect. 121, 197–204.
- Harlan, S.L., Chowell, G., Yang, S., Petitti, D.B., Morales Butler, E.J., Ruddell, B.L., Ruddell, D.M., 2014. Heat-related deaths in hot cities: estimates of human tolerance to high temperature thresholds. Int. J. Environ. Res. Public Health 11, 3304–3326.
- Hoffman, J.S., Shandas, V., Pendleton, N., 2020. The effects of historical housing policies on resident exposure to intra-urban heat: a study of 108 US urban areas. Climate 8.
- House-Peters, L., Pratt, B., Chang, H., 2010. Effects of urban spatial structure, sociodemographics, and climate on residential water consumption in Hillsboro, Oregon. J. Am. Water Resour. Assoc. 46, 461–472.
- Hsu, A., Sheriff, G., Chakraborty, T., Manya, D., 2021. Disproportionate exposure to urban heat island intensity across major US cities. Nat. Commun. 12, 2721.
- Huang, G., Zhou, W., Cadenasso, M.L., 2011. Is everyone hot in the city? Spatial pattern of land surface temperatures, land cover and neighborhood socioeconomic characteristics in Baltimore, MD. J. Environ. Manag. 92, 1753–1759.
- Huang, S., Tang, L., Hupy, J.P., Wang, Y., Shao, G., 2020. A commentary review on the use of normalized difference vegetation index (NDVI) in the era of popular remote sensing. J. For. Res. 32, 1–6.
- Ibsen, P.C., Santiago, L.S., Shiflett, S.A., Chandler, M., Jenerette, G.D., 2023. Irrigated urban trees exhibit greater functional trait plasticity compared to natural stands. Biol. Lett. 19, 20220448.
- Imhoff, M.L., Zhang, P., Wolfe, R.E., Bounoua, L., 2010. Remote sensing of the urban heat island effect across biomes in the continental USA. Remote Sens. Environ. 114, 504–513.
- Jamali, F.S., Khaledi, S., Razavian, M.T., 2021. Seasonal impact of urban parks on land surface temperature (LST) in semi-arid city of Tehran. Int. J. Urban Sustain. Dev. 13, 248–264.
- James, P., Hart, J.E., Banay, R.F., Laden, F., 2016. Exposure to greenness and mortality in a nationwide prospective cohort study of women. Environ. Health Perspect. 124, 1344–1352.
- Jenerette, G.D., Harlan, S.L., Stefanov, W.L., Martin, C.A., 2011. Ecosystem services and urban heat riskscape moderation: water, green spaces, and social inequality in Phoenix, USA. Ecol. Appl. 21, 2637–2651.
- Jenerette, G.D., Miller, G., Buyantuev, A., Pataki, D.E., Gillespie, T.W., Pincetl, S., 2013. Urban vegetation and income segregation in drylands: a synthesis of seven metropolitan regions in the southwestern United States. Environ. Res. Lett. 8.
- Jenerette, G.D., Clarke, L.W., Avolio, M.L., Pataki, D.E., Gillespie, T.W., Pincetl, S., Nowak, D.J., Hutyra, L.R., McHale, M., McFadden, J.P., Alonzo, M., 2016. Climate tolerances and trait choices shape continental patterns of urban tree biodiversity. Glob. Ecol. Biogeogr. 25, 1367–1376.
- Jennings, V., Johnson Gaither, C., Gragg, R.S., 2012. Promoting environmental justice through urban green space access: a synopsis. Environ. Justice 5, 1-7.
- Jennings, V., Browning, M.H.E.M., Rigolon, A., 2019. Urban Green Space at the Nexus of Environmental Justice and Health Equity. Urban Green Spaces, pp. 47–69. Jesdale, B.M., Morello-Frosch, R., Cushing, L., 2013. The racial/ethnic distribution of heat risk-related land cover in relation to residential segregation. Environ. Health Perspect. 121, 811–817.
- Jin, J., Gergel, S.E., Lu, Y., Coops, N.C., Wang, C., 2019. Asian cities are greening while some north American cities are browning: long-term greenspace patterns in 16 cities of the Pan-Pacific region. Ecosystems 23, 383–399.
- Jombo, S., Adam, E., Byrne, M.J., Newete, S.W., 2022. Assessing the intraurban differences in vegetation coverage and surface climate in a heterogeneous area. Trans. R. Soc. S. Afr. 77. 1–10.

Keenan, J.M., Hill, T., Gumber, A., 2018. Climate gentrification: from theory to empiricism in Miami-Dade County, Florida. Environ. Res. Lett. 13.

Kephart, L., 2022. How racial residential segregation structures access and exposure to greenness and green space: a review. Environ. Justice 15, 204-213.

Kirschbaum, M.U., 2004. Direct and indirect climate change effects on photosynthesis and transpiration. Plant Biol. (Stuttg.) 6, 242-253.

Konarska, J., Uddling, J., Holmer, B., Lutz, M., Lindberg, F., Pleijel, H., Thorsson, S., 2016. Transpiration of urban trees and its cooling effect in a high latitude city. Int. J. Biometeorol. 60, 159–172.

Krafft, J., Fryd, O., 2016. Spatiotemporal patterns of tree canopy cover and socioeconomics in Melbourne. Urban For. Urban Green. 15, 45–52.

Lantz, B., 2013. The large sample size fallacy. Scand. J. Caring Sci. 27, 487-492.

Larson, K.L., Brumand, J., 2014. Paradoxes in landscape management and water conservation: examining neighborhood norms and instititional forces. Cities Environ. (CATE) 7.

Lemoine-Rodriguez, R., Inostroza, L., Zepp, H., 2022. Does urban climate follow urban form? Analysing intraurban LST trajectories versus urban form trends in 3 cities with different background climates. Sci. Total Environ. 830, 154570.

Leong, M., Dunn, R.R., Trautwein, M.D., 2018. Biodiversity and socioeconomics in the city: a review of the luxury effect. Biol. Lett. 14.

Li, D., Sun, T., Liu, M., Yang, L., Wang, L., Gao, Z., 2015. Contrasting responses of urban and rural surface energy budgets to heat waves explain synergies between urban heat islands and heat waves. Environ. Res. Lett. 10.

Li, M., Yao, J., Guan, J., Zheng, J., 2021. Observed changes in vapor pressure deficit suggest a systematic drying of the atmosphere in Xinjiang of China. Atmos. Res. 248.

Liang, L.L., Anderson, R.G., Shiflett, S.A., Jenerette, G.D., 2017. Urban outdoor water use and response to drought assessed through mobile energy balance and vegetation greenness measurements. Environ. Res. Lett. 12.

Litvak, E., Manago, K.F., Hogue, T.S., Pataki, D.E., 2017. Evapotranspiration of urban landscapes in Los Angeles, California at the municipal scale. Water Resour. Res. 53, 4236–4252.

Liu, Y., Peng, J., Wang, Y., 2018. Efficiency of landscape metrics characterizing urban land surface temperature. Landsc. Urban Plan. 180, 36-53.

Liu, H., Huang, B., Gao, S., Wang, J., Yang, C., Li, R., 2021. Impacts of the evolving urban development on intra-urban surface thermal environment: evidence from 323 Chinese cities. Sci. Total Environ. 771, 144810.

Locke, D.H., Grove, J.M., 2014. Doing the hard work where it's easiest? Examining the relationships between urban greening programs and social and ecological characteristics. Appl. Spat. Anal. Policy 9, 77–96.

Loveland, T.R., Dwyer, J.L., 2012. Landsat: building a strong future. Remote Sens. Environ. 122, 22-29.

Manavvi, S., Rajasekar, E., 2023. Assessing thermal comfort in urban squares in humid subtropical climate: a structural equation modelling approach. Build. Environ. 229.

McCarthy, H.R., Pataki, D.E., 2010. Drivers of variability in water use of native and non-native urban trees in the greater Los Angeles area. Urban Ecosyst. 13, 393.414

McPhearson, T., Feller, M., Felson, A., Karty, R., Lu, J.W.T., 2010. Assessing the effects of the urban forest restoration effort of MillionTreesNYC on the structure and functioning of New York City ecosystems. Cities Environ. (CATE) 3.

Miller, D.L., Alonzo, M., Roberts, D.A., Tague, C.L., McFadden, J.P., 2020. Drought response of urban trees and turfgrass using airborne imaging spectroscopy. Remote Sens. Environ. 240.

Mishra, V., Ambika, A.K., Asoka, A., Aadhar, S., Buzan, J., Kumar, R., Huber, M., 2020. Moist heat stress extremes in India enhanced by irrigation. Nat. Geosci. 13, 722–728.

Morello-Frosch, R., Zuk, M., Jerrett, M., Shamasunder, B., Kyle, A.D., 2011. Understanding the cumulative impacts of inequalities in environmental health: implications for policy. Health Aff. (Millwood) 30, 879–887.

Murage, P., Kovats, S., Sarran, C., Taylor, J., McInnes, R., Hajat, S., 2020. What individual and neighbourhood-level factors increase the risk of heat-related mortality? A case-crossover study of over 185,000 deaths in London using high-resolution climate datasets. Environ. Int. 134, 105292.

Oke, T.R., Stewart, I.D., 2012. Local climate zones for urban temperature studies. Bull. Am. Meteorol. Soc. 93, 1879–1900.

Oudin Åström, D., Forsberg, B., Ebi, K.L., Rocklöv, J., 2013. Attributing mortality from extreme temperatures to climate change in Stockholm, Sweden. Nat. Clim. Chang. 3, 1050–1054.

Pataki, D., McCarthy, H.R., Litvak, E., Pincetl, S., 2011a. Transpiration of urban forests in the Los Angeles metropolitan area. Ecol. Appl. 21, 661-677.

Pataki, D.E., Boone, C.G., Hogue, T.S., Jenerette, G.D., McFadden, J.P., Pincetl, S., 2011b. Socio-ecohydrology and the urban water challenge. Ecohydrology 4, 341–347.

Pettorelli, N., Ryan, S., Mueller, T., Bunnefeld, N., Jedrzejewska, B., Lima, M., Kausrud, K., 2011. The normalized difference vegetation index (NDVI): unforeseen successes in animal ecology. Clim. Res. 46, 15–27.

Pincetl, S., Gillespie, T.W., Pataki, D.E., Porse, E., Jia, S., Kidera, E., Nobles, N., Rodriguez, J., Choi, D.-A., 2019. Evaluating the effects of turf-replacement programs in Los Angeles. Landsc. Urban Plan. 185, 210–221.

Polydoros, A., Mavrakou, T., Cartalis, C., 2018. Quantifying the trends in land surface temperature and surface urban heat island intensity in Mediterranean cities in view of smart urbanization. Urban Sci. 2.

Purio, M.A., Yoshitake, T., Cho, M., 2022. Assessment of intra-urban heat island in a densely populated city using remote sensing: a case study for Manila City. Remote Sens. 14.

Qi, Y., Li, H., Pang, Z., Gao, W., Liu, C., 2022. A case study of the relationship between vegetation coverage and urban heat island in a coastal city by applying digital twins. Front. Plant Sci. 13, 861768.

Qiu, G.-Y., Li, H.-Y., Zhang, Q.-T., Chen, W., Liang, X.-J., Li, X.-Z., 2013. Effects of evapotranspiration on mitigation of urban temperature by vegetation and urban agriculture. J. Integr. Agric. 12, 1307–1315.

Quesnel, K.J., Ajami, N., Marx, A., 2019. Shifting landscapes: decoupled urban irrigation and greenness patterns during severe drought. Environ. Res. Lett. 14. Reid, C.E., O'Neill, M.S., Gronlund, C.J., Brines, S.J., Brown, D.G., Diez-Roux, A.V., Schwartz, J., 2009. Mapping community determinants of heat vulnerability.

Environ. Health Perspect. 117, 1730–1736.

Ren, T., Zhou, W., Wang, J., 2021. Beyond intensity of urban heat island effect: a continental scale analysis on land surface temperature in major Chinese cities. Sci. Total Environ. 791, 148334.

Romolini, M., Grove, J.M., Locke, D.H., 2013. Assessing and comparing relationships between urban environmental stewardship networks and land cover in Baltimore and Seattle. Landsc. Urban Plan. 120, 190–207.

Schwarz, K., Fragkias, M., Boone, C.G., Zhou, W., McHale, M., Grove, J.M., O'Neil-Dunne, J., McFadden, J.P., Buckley, G.L., Childers, D., Ogden, L., Pincetl, S., Pataki, D., Whitmer, A., Cadenasso, M.L., 2015. Trees grow on money: urban tree canopy cover and environmental justice. PLoS One 10, e0122051.

Shahfahad, A.A., Bindajam, M.W., Naikoo, J.P., Horo, J., Mallick, M., Rihan, M.D., Malcoti, S. Talukdar, Rahman, R., Rahman, A., 2023. Response of soil moisture and vegetation conditions in seasonal variation of land surface temperature and surface urban heat island intensity in sub-tropical semi-arid cities. Theor. Appl. Climatol. 153, 367–395.

Shih, W.-Y., 2022. Socio-ecological inequality in heat: the role of green infrastructure in a subtropical city context. Landsc. Urban Plan. 226.

Shokry, G., Connolly, J.J.T., Anguelovski, I., 2020. Understanding climate gentrification and shifting landscapes of protection and vulnerability in green resilient Philadelphia. Urban Clim. 31.

Siddiqui, A., Kushwaha, G., Nikam, B., Srivastav, S.K., Shelar, A., Kumar, P., 2021. Analysing the day/night seasonal and annual changes and trends in land surface temperature and surface urban heat island intensity (SUHII) for Indian cities. Sustain. Cities Soc. 75.

Slette, I.J., Post, A.K., Awad, M., Even, T., Punzalan, A., Williams, S., Smith, M.D., Knapp, A.K., 2019. How ecologists define drought, and why we should do better. Glob. Chang. Biol. 25, 3193–3200.

Son, J.Y., Lane, K.J., Lee, J.T., Bell, M.L., 2016. Urban vegetation and heat-related mortality in Seoul, Korea. Environ. Res. 151, 728-733.

Tayyebi, A., Jenerette, G.D., 2016. Increases in the climate change adaption effectiveness and availability of vegetation across a coastal to desert climate gradient in metropolitan Los Angeles, CA, USA. Sci. Total Environ. 548-549, 60–71.

Tian, P., Li, J., Cao, L., Pu, R., Wang, Z., Zhang, H., Chen, H., Gong, H., 2021. Assessing spatiotemporal characteristics of urban heat islands from the perspective of an urban expansion and green infrastructure. Sustain. Cities Soc. 74.

USGS, U. S. G. S, 2021a. Landsat 4-7 Collection 2 (C2) Level 2 Science Product (L2SP) Guide. LSDS-1618, Sioux Falls, South Dakota.

USGS, U. S. G. S, 2021b. Landsat 8-9 Calibration and Validation (Cal/Val) Algorithm Description Document (ADD). LSDS-1747, Sioux Falls, South Dakota.

Vahmani, P., Hogue, T.S., 2015. Urban irrigation effects on WRF-UCM summertime forecast skill over the Los Angeles metropolitan area. J. Geophys. Res. Atmos. 120, 9869–9881.

Varquez, A.C.G., Kanda, M., 2018. Global urban climatology: a meta-analysis of air temperature trends (1960–2009). npj Clim. Atmos. Sci. 1.

Vasey, M.C., Parker, V.T., Holl, K.D., Loik, M.E., Hiatt, S., 2014. Maritime climate influence on chaparral composition and diversity in the coast range of Central California. Ecol. Evol. 4, 3662–3674.

Venter, Z.S., Shackleton, C.M., Van Staden, F., Selomane, O., Masterson, V.A., 2020. Green apartheid: urban green infrastructure remains unequally distributed across income and race geographies in South Africa. Landsc. Urban Plan. 203.

Vicente-Serrano, S.M., Beguería, S., López-Moreno, J.I., 2010. A multiscalar drought index sensitive to global warming: the Standardized Precipitation Evapotranspiration Index. J. Clim. 23, 1696–1718.

Voogt, J.A., Oke, T.R., 2003. Thermal remote sensing of urban climates. Remote Sens. Environ. 86, 370-384.

Wan, Z., Wang, P., Li, X., 2004. Using MODIS land surface temperature and normalized difference vegetation index products for monitoring drought in the southern Great Plains, USA. Int. J. Remote Sens. 25, 61–72.

Watkins, S.L., Gerrish, E., 2018. The relationship between urban forests and race: a meta-analysis. J. Environ. Manag. 209, 152-168.

Wetherley, E.B., McFadden, J.P., Roberts, D.A., 2018. Megacity-scale analysis of urban vegetation temperatures. Remote Sens. Environ. 213, 18-33.

Whitley, R., Taylor, D., Macinnis-Ng, C., Zeppel, M., Yunusa, I., O'Grady, A., Froend, R., Medlyn, B., Eamus, D., 2013. Developing an empirical model of canopy water flux describing the common response of transpiration to solar radiation and VPD across five contrasting woodlands and forests. Hydrol. Process. 27, 1133–1146.

Winbourne, J.B., Jones, T.S., Garvey, S.M., Harrison, J.L., Wang, L., Li, D., Templer, P.H., Hutyra, L.R., 2020. Tree transpiration and urban temperatures: current understanding, implications, and future research directions. BioScience 70, 576–588.

Wong, D.W., Sun, M., 2013. Handling data quality information of survey data in GIS: a case of using the American community survey data. Spat. Demogr. 1, 3–16. Wu, W., Li, L., Li, C., 2021. Seasonal variation in the effects of urban environmental factors on land surface temperature in a winter city. J. Clean. Prod. 299.

Yang, Q., Huang, X., Yang, J., Liu, Y., 2021. The relationship between land surface temperature and artificial impervious surface fraction in 682 global cities: spatiotemporal variations and drivers. Environ. Res. Lett. 16.

Yin, Y., He, L., Wennberg, P.O., Frankenberg, C., 2023. Unequal exposure to heatwaves in Los Angeles: impact of uneven green spaces. Sci. Adv. 9.

Yuan, F., Bauer, M.E., 2007. Comparison of impervious surface area and normalized difference vegetation index as indicators of surface urban heat island effects in Landsat imagery. Remote Sens. Environ. 106, 375–386.

Zhao, S., Cong, D., He, K., Yang, H., Qin, Z., 2017. Spatial-temporal variation of drought in China from 1982 to 2010 based on a modified temperature vegetation drought index (mTVDI). Sci. Rep. 7, 17473.

Zhao, D., Lei, Q., Shi, Y., Wang, M., Chen, S., Shah, K., Ji, W., 2020. Role of species and planting configuration on transpiration and microclimate for urban trees. Forests 11.

Zhou, W., Huang, G., Cadenasso, M.L., 2011. Does spatial configuration matter? Understanding the effects of land cover pattern on land surface temperature in urban landscapes. Landsc. Urban Plan. 102, 54–63.

Zhu, Z., 2019. Science of Landsat analysis ready data. Remote Sens. 11.

Zipper, S.C., Schatz, J., Kucharik, C.J., Loheide, S.P., 2017. Urban heat island-induced increases in evapotranspirative demand. Geophys. Res. Lett. 44, 873-881.

Ziter, C.D., Pedersen, E.J., Kucharik, C.J., Turner, M.G., 2019. Scale-dependent interactions between tree canopy cover and impervious surfaces reduce daytime urban heat during summer. Proc. Natl. Acad. Sci. U. S. A. 116, 7575–7580.